UNIVERSITÀ DEGLI STUDI DI PADOVA

UNIVERSITA' DEGLI STUDI DI PADOVA

Dipartimento di Ingegneria Industriale DII

Corso di Laurea magistrale in Ingegneria dei materiali

3D printing and characterization of bio-glass Wollastonite-Diopside

Relatore:

Prof. Paolo Colombo

Laureanda:

Baesso Ilaria

Anno Accademico 2017/2018

“Vivi pericolosamente!
Vivi pericolosamente, se vuoi sviluppare la tua personalità.”
Nietzsche

Abstract

In the present thesis the study in terms of physical and mechanical characteristics as well as bioactive behavior on an innovative glass-ceramic is introduced .
Two different compositions of this material are proposed: the eutectic composition and another one in wich a flux is added.

This material belongs to a Wollasonite-Diopside binary system. Both materials (wollastonite and diopside) have already been studied individually showing, both of them, good features of bioactivity besides the good mechanical properties.

The first part of the work focuses on the physical and mechanical characterization of the innovative material while the second part intends to analyze its *in vitro* degradation and bioactivity.

Specifically, physical and mechanical analysis aim to characterize structures realized by means of powder-based 3D printing. A detailed comparison between pressed and printed tablets will be shown as well as the study of shape maintenance of printed scaffolds.

Physical studies include DTA and hot stage microscopy analysis, evaluation of shrinkage due to the heat treatments as well as density and porosity measurements.

Particular attention is paid to the heat treatments as they influence formation of crystalline phases and shape maintenance of samples.

Mechanical characterization is based on results from ball on three balls tests analyzed by means of Weibull statistics.

In the second part of the work the two compositions of the material under analysis were compared to a further material with well kown bioactive behavior.

Degradation and bioactivity tests are carried out by ion release measurements after immersion of samples in TRIS-HCl solution and SBF respectively.

The last part of the work consists in the imaging of samples surfaces after immersion in SBF by means of scanning electron microscopy.

Table of contents

List of tables

List of figures

Introduction

As it is already known, some polymers, ceramics and metals have widely been used to create different types of medical devices such as prosthesis or sutures and, as a consequence, it has been possible to repair many different kinds of injuries. In the last forty years, the interest in biomaterials has increased a lot and many researches on this topic have been carried out, this is one of them.

Some glasses, ceramics and glass-ceramics play an important role in the biomedical field particularly with bone tissue engineering matters. What makes this class of materials interesting is their capability to create a strong bond with bones without the intervention of surrounding fibrous tissue. The bone-bonding mechanism is peculiar and involves necessarily the formation, in the presence of human physiological environment, of an apatite-like layer on the surface of the material. This layer is equivalent chemically and structurally to the mineral phase that is naturally present in the human bones and provides the bonding interface with them.

Bioglass® is the first material that has been found to bond to the living bone (by Larry L. Hench, 1960s) and since that discovery many other similar materials have been developed such as sintered hydroxyhapatite (HA), sintered β-tricalcuimphopsphate (TCP), wollastonite-apatite (WA), wollasonite-diopside (WD). Applications of these materials nowadays include for example replacements for hips, knees, teeth, tendons, stabilization of the jaw bone, bone fillers of defects or after tumor surgery. Ceramics are also used to replace parts of the cardiovascular system, especially heart valves. Special formulations of glasses are also used therapeutically for the treatment of tumors, some devices, for example, are implanted around malignant tumors and placed under an alternating magnetic field in order to heat the tumor up to a temperature of 43°C.

Most applications are achieved by means of powder even if many studies are focusing lately on realization of scaffolds, namely, tailored structures (realized, for examples, by means of additive manufacturing) that can at the same time mimic the porous structure of the natural bone and provide higher mechanical properties compared to powders. Moreover, it must be underlined that an interconnected porous structure is essential in order to provide sufficient space for cell migration, adhesion and the ingrowth of new bone tissue. The most similar the material is to the natural environment, in fact, the easiest will be the tissue regeneration on it.

The present thesis will introduce the work carried out at BAM from April to October 2017. The main aim of the entire work was to perform dissolution and bioactivity analysis on wollastonite-diopside glass-ceramic. Some other experiments have been done before these analyses in order to identify the best heat treatment for crystallization of the material. Measurements of density, porosity and mechanical properties have also been conducted.

Chapter 1 : Biomaterials and bioactive materials

1.1 Biomaterials and bioceramics

Before getting into the details of the present thesis, it is important to clarify what biomaterials means and which are all the subclasses.

The most accepted definition of biomaterials is currently the one employed by the American National Institute of Health that describes biomaterial as *'any substance or combination of substances, other than drugs, synthetic or natural in origin, which can be used for any period of time, which augments or replaces partially or totally any tissue, organ or function of the body, in order to maintain or improve the quality of life of the individual'*[1]. All materials, therefore, elicit a response from the host tissue and the most important requirement for a biomaterial is its lack of toxicity.

Based on the reaction of the tissue to the biomaterial, these are classified into three distinct categories:

1. *Biotolerant Materials*: which are separated from bone tissue by a layer of fibrous tissue;
2. *Bioactive materials*: which have the property of establishing chemical bonds with bone tissue, known as osteointegration. The collagen and mineral phase of the adjacent bone is deposited directly on the implant surface;
3. *Bioinert Materials*: in this class, it is possible, under certain conditions, to have direct contact with the adjacent bone tissue. No chemical reactions shall occur between the implant and the tissue.

The essential feature that some glass, ceramics and glass-ceramics have in common is their bioactivity (capability to bond directly and strongly to bones), that metal, some other ceramics (as alumina and zirconia) and polymers do not have. Indeed, what is more common is that the material produce an interfacial mechanism by which a fibrous tissue is formed in order to isolate the implant from the host.

The common characteristic of all bioactive implants, is the formation of a hydroxy-carbonate apatite (HCA) layer on their surface when implanted (the mechanism involves the release of calcium and sodium ions from the glass). The HCA phase is equivalent in composition and structure to the mineral phase of bone. This layer grows as polycrystalline agglomerates. Collagen fibrils are incorporated within the agglomerates, thereby, binding the inorganic implant surface to the organic constituents of tissues. Thus, the interface between a bioactive implant and bone is nearly identical to the naturally-occurring interfaces between bone and tendons and ligaments. It has been found also that the strength of that interface is by far higher than that of the bone and the material. One experiment made by Kokubo[2]

demonstrated, indeed, that a couple of rectangular specimens ($4\times4\times26$ mm^3) of a bioactive material brought in contact with each other and immersed into the simulated body fluid were so tightly bonded that, after one month, they could not be separated by manual force.

Then it is possible to distinguish two different classes of bioactivity: A and B[3]. Class A bioactivity leads to both osteoconductivity (*i.e.* bone migrates along an interface) and osteostimulation as a consequence of rapid reactions on the bioactive glass surface. The surface reactions involve ionic dissolution of critical concentrations of soluble Si and P species and Ca and Na ions that give rise to both intracellular and extracellular responses at the interface of the glass with its physiological environment. Class B bioactivity occurs when only osteoconduction is present. This limited tissue response is due to slower surface reactions and minimal ionic release. Only extracellular responses occur at the interface of Class B bioactive tissue interfaces.

Another important distinction is based on the stability of the material in contact with the human body: there are *biostable* and *bioresorbable* materials. Biostable materials cannot be modified once grafted by the body environment while bioresorbable materials can be degraded and adsorbed by the body. Thus, a resorbable biomaterial must be of a composition that can be chemically degraded by body fluids or easily digested by macrophages. The degradation products must be chemical compounds that are not toxic and can be easily disposed of without damage to cells.

Combination of bioactivity and bioresorbability allows to create structures on which new tissue can grow replacing the material so that further surgery can be avoided. One of the main limits, indeed, of the typical metal and polymeric implants is the requirement of more surgery or substitutions after implantation.

The main challenge nowadays is to find the perfect compromise between high mechanical properties, bioactivity and suitable adsorption rate. For instance, glass is too weak for load-bearing applications but glass phase is essential for bioactivity. So, glass-ceramics are promising materials to satisfy all the requirements as they have quite higher mechanical properties. Other possibilities to overcome the problem of glass's weakness is to create coatings of bioactive materials on substrates with sufficient mechanical strength as metals o polymers[4].

One of the most important glass-ceramic for biomedical applications was developed by Kokubo and it is known as Cerabone®. It consists of crystalline apatite and wollastonite in a $MgO\text{-}CaO\text{-}SiO_2$ glassy matrix. Apatite-wollastonite glass-ceramic has also been developed as coating for titanium alloys[5]. Another important glass-ceramic is known as Ceravital® and it contains a glassy phase and an apatite crystalline phase.

In order to better understand the present thesis it is worth to give an overview on Bioglasses, calcium-phosphate ceramics and the two materials used in the experiments: wollastonite-apatite (WA) and wollastonite-diopside (WD) glass-cermics.

1.2 Bioglasses

It was discovered by Hence and colleagues in 1970 that bone can bond chemically to certain glass compositions. The base components in most bioactive glasses are SiO_2, Na_2O, CaO, and P_2O_5. The first and most famous Bioglass® is known as 4S5S (45% SiO_2, 24.5% Na_2O, 24.4% CaO and 6% P_2O_5, in weight percent).

The primary advantage of bioactive glasses is their rapid rate of surface reaction, which leads to fast tissue bonding. These materials, moreover, can bond with both bone and soft tissue. It has been demonstrated by Dr. June Wilson[6] that only if the interface is immobile and only if the glass composition allows rapid reaction rates, the material can bond to soft tissue. When the composition, for example, exceeds 52% by weight of SiO_2 the material can bond exclusively to bone.

It is possible to undestrand and predict the behavior of different glasses composition looking at the diagram showed below (Figure 1-1).

From that figure it is easy to undestrand that bioglasses able to bond to soft tissue are only the ones included in the S region. It can be noted, also, that for contents of SiO_2 above 60% the material is bioinert (*i.e.* does not bond to bone).

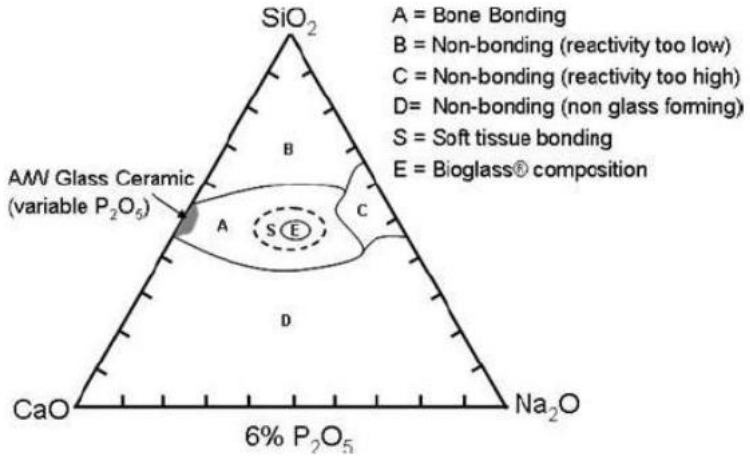

Figure 1-1: Compositional dependence in weight percent of bone bonding and soft-tissue bonding of bioactive glasses and glass-ceramics.

Another aspect that makes bioactive glasses different from other bioactive ceramics and glass-ceramics is the possibility to tailor glasses with specific properties to a particular clinical application. This is also possible with some glass-ceramics, but their heterogeneous microstructure restricts their versatility.

On the other hand, the main disadvantages of Bioglass®, are the mechanical weakness and the low fracture toughness, both due to the amorphous structure. The typical range of bending

strength of bioglasses is 40-60 MPa while for cortical bones it is within the range: 50-150 MPa, this makes these materials not suitable for load-bearing applications. Its low strength does not compromise, however, when applying it as coating, buried implants or in low-loaded and compressively loaded devices.

Two decades after Bioglass® discovery, a new silicate-based glass was developed to overcome its processing limitations. The new composition, termed 13-93 glass, is based on the 45S5 Bioglass® composition, but has higher silica content (53 wt%) and K_2O and MgO as additional network modifiers. This glass showed an enhanced viscous flow behavior, less tendency to crystallize, and when in the form of porous scaffold, it exhibited porosity content and mechanical properties comparable to those of cancellous bone. The bioactive behavior of the 13-93 glass was demonstrated by the formation of an HA layer on the surface of 13-93-derived scaffold surface, in less than 7 days of immersion in SBF, indicating its potential of bonding to bone. Furthermore, *in vivo* studies demonstrated the ability of the 13-93 formulation in supporting tissue ingrowth.

Worldwide many researchers have used the SiO_2-Na_2O-CaO-P_2O_5 system and particularly its ancestor (the 45S5 bioactive glass), as template materials to develop new silica-based formulations. The possibility to tailor the glass properties, altering the main formulation by using different oxides, is currently an open challenge for the design of more complex compositional systems.
The table below shows the compositions of some silicate glasses mainly investigated in literature[7].

Table 1-1:Compositions of main silicate bioglasses

Compositions (wt%)	**4S5S**	**13-93**	**58S**	**70S30C**	**77S**	**13-93B1**
SiO	45	53	58.2	71.4	80	34.4
KO	-	12	-	-	-	11.7
NaO	24.5	6	-	-	-	5.8
MgO	-	5	-	-	-	4.9
PO	6	4	9.2	-	-	3.8
BO	-	-	-	-	-	19.9
CaO	24.5	20	32.6	16	16	19.5

1.3 Calcium phosphate ceramics

Due to the similarity with the mineral component of human bone, calcium phosphate ceramics (CaP) have been extensively used as biomaterials for the repair and regeneration of bone tissue for the last 30years.

There are different forms of CaP ceramics that are most commonly investigated in the field of BTE are: HA, β -tricalcium phosphate (β-TCP) and biphasic calcium phosphate (BCP).

HA is the CaP ceramic most widely used because it shares chemical similarities to inorganic component of bone tissue. Although it is not highly soluble, it supports nucleating sites for the precipitation of apatite crystals in culture medium.

TCP is a biodegradable bioceramic with a Ca/P molar ratio of 1.5. It exists in two different phases, which are α and β. Both phases are less stable than HA and therefore more soluble in aqueous environments. Despite their similarities in chemical composition, α-TCP is more soluble than β-TCP, but from a clinical perspective β-TCP is osteoconductive and osteoinductive, and hence more widely used in bone regeneration than α-TCP.

Depending on the situation, it might be necessary for an implant to resorb slowly before being replaced by the host tissue. For this reason, a combination of HA and TCP has been investigated, in which the higher TCP/HA ratio leads to a higher dissolution rate. CaP ceramics represent a class of tunable biomaterials with exclusive properties, they are used in different areas of the human skeleton (*e.g.* treatment of bone defects, maxillofacial applications, spinal fusion and bone augmentation)[8]. However, how calcium phosphate properties help osteoinductivity and osteoconductivity are still unanswered questions, for this reason they are a class of materials still actively being researched.

1.4 Wollastonite-Apatite glass-ceramics

WA glass-ceramics is probably the most important example of glass-ceramic for biomedical use. It was synthesized by T. Kokubo by the initial idea to recreate something like the natural bone, that is, a microcomposite in which an assembly of apatite small particles is effectively reinforced by collagen fibres. The main aim of the project was to improve the mechanical properties of bioglasses and the result was an assembly of apatite small particles reinforced with β-wollastonite ($CaO.SiO_2$) having a silicate chain structure. This material showed not only high bioactivity but, above all, a fairly high mechanical strength which decreased slowly, even under load bearing condition in the body.

The nominal composition of the material is MgO 4,6%, CaO 44,9%, SiO_2 34,2%, P_2O_5 16.3%, CaF_2 0.5% by weight ratio.

It has been found that the bending strength of this material was about 200MPa in air environment that is higher than the 160 MPa of human cortical bone. This high value has

been attributed to the high fracture toughness which increases with the precipitation of β-wollastonite. Some mechanical tests were taken also on the material soaked in SBF and it showed only a small decrease in mechanical strength. Moreover, when the material was placed in SBF without being loaded, it rather showed an increase in mechanical strength. The increase in strength with soaking might be attributed to crack blunting at the surface of the glass-ceramic that might be caused by the apatite deposition on the glass-ceramic in the SBF. This result indicated that practical life-time of this glass-ceramic AW could have been much more prolonged that the estimated one (It is possible, indeed, to predict the life-time, i.e. time of failure, of glasses and glass-ceramics in aqueous environment by an equation)[9].

Glass-ceramic AW containing crystalline apatite and wollastonite have been used as artificial vertebrae, intervertebral spacers, iliac spacers, bone fillers by the name of Cerabone® (Figure 1-2). Applications as femoral and tibias bones are however not suitable since its fracture toughness is not so high as that of human cortical bone (2 and 6 MPa $m^{1/2}$ respectively) and its elastic modulus is not so low as the one of cortical bone (118 and 30 GPa respectively).

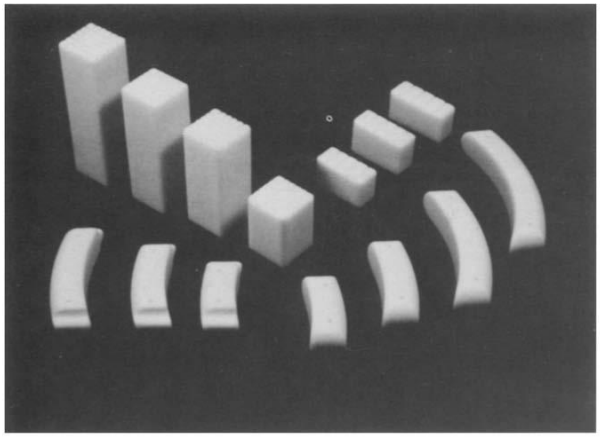

Figure 1-2: Iliac spacers (left), artificial vertebae (middle top), spinous process spacers (middle bottom) and invertrebal spacers (right) of Cerabone®.

Another advantage of this material is that, by the introduction of MgO in the composition, the silica layer between the surface and the apatite layer, that was observed with the Bioglass, is not producted in body environment. Indeed, that layer is not desirable as its mechanical strength is quite law and it compromises the entire mechanical performance. It has been demonstrated that when CaO is replaced with MgO the thickness of the silica gel decrease and that for glass of molar composition of 10 % MgO, 40% CaO and 50% SiO_2 the apatite layer is in direct contact with the glass without the intervention of the Silica layer even after immersion in SBF.

1.5 Wollastonite-Diopside glass-ceramics

Following the same ideas by which WA glass ceramic was developed, in 2004 Ohtsuki et al. synthetized a new glass-ceramic with the molar composition of 10 % MgO, 40% CaO and 50% SiO2. The parent glass was obtained by a traditional melt-quenching technique and

precipitation of the crystalline phases wollastonite and diopside was observed after heat treatment at temperatures above 900°C. In this material, therefore, the properties of the two different ceramics are exploited[10].

Wollastonite ceramic has high thermal and mechanical properties and its bioactivity permits also biomedical applications. It is possible to obtain wollastonite ceramics from coal fly ash of thermal power plant and glass cullet with mechanical strength suitable for applications as industrial floor covering, abrasion resistant linings and high temperatures insulators[11].

Its main problem is the high rate of dissolution in body environment that can compromise the performances as medical device.

Realization of composites could help to overcome the problem associated with the high dissolution rate.

Diopside, for example, has a lower dissolution rate and fairly high mechanical properties. It has been proved, indeed, that the compressive strength of diopside scaffolds prepared using the polymer sponge template is higher than those of bioglass and $CaSiO_3$ scaffolds prepared with the same method and that these properties decrease only by 30% after soaking in SBF for 14 days, compared to a decrease of 54% and 60% in the strength of Bioglass and $CaSiO_3$ scaffolds. These data suggest diopside's superiority to traditional bioceramics in bone repair applications. The better mechanical behavior compared with bioglass and wollasonite is due to two different potential reasons. The first reason is linked to the different composition: diopside is a Mg-containing compound and Mg atoms can occupy the positions of Ca atoms forming Mg-O bondings that have higher bonding energy resulting in a more stable crystal structure. The other reason is the difference in sintering procedures, diopside scaffolds can be processed at temperatures of about 1330°C resulting in formation of very highly dense pore walls while, bioglass, for example, cannot be processed at temperatures above 700°C in order to avoid the formation of undesired crystal phase[12].

Some studies on the composite Wollastonite-Diopside have been carried out since its discovery but most of times the production technique was different. It has been possible, indeed, to obtain it from preceramic polymers that is a different way compared to the procedure used for the material described in the present thesis. It has been demonstrated, that the polymer-derived glass-ceramic has a good bioactivity as an apatite-like layer was detected by means of XRD and FTIR techniques after soaking in SBF for 7 days and that the crystalline fraction influences the degradation rate: the higher the crystalline fraction, the lower the rate of degradation. It has been showed, moreover, that the material is not citotoxic and this makes it a good candidate to be used in tissue engineering[13].

1.6 Bone bonding mechanism and apatite formation

It has been demonstrated that the essential requirement for an artificial material to bond to living bone is the formation of the apatite layer on their surface in the body.

The apatite layer can be reproduced on the surface of bioactive glass and glass-ceramics even in an acellular simulated body fluid (SBF) with ion concentration nearly equal to those of human blood plasma. The structural and compositional characteristic are very similar to those of the apatite in the bone and bone-production cells, osteoblasts, can preferentially proliferate on this apatite layer and differentiate to produce the apatite and collagen. These biological apatite and collagen soon fully occupy the space in the bioactive material and come to direct contact with the surface apatite layer and when this occurs, a tight chemical bond is formed between the bone apatite and the surface apatite.

Even if the examination of apatite formation in SBF is only a preliminary test, it is useful for predicting the *in-vivo* bone bioactivity of the material and the number of animals used for *in-vivo* tests as well as the duration of animal experiments can be remarkably reduced.

It has been believed for a long period that the P_2O_5 was the essential component for a material to be bioactive but later it was demonstrated that even P_2O_5-free glasses and glass-ceramics form the bone like apatite layer on their surface in SBF. The CaO, SiO_2-based glasses release mainly the calcium ions into SBF whereas the CaO,P_2O_5-based glasses release mainly the phosphate ions. Both of these ions are components of SBF and their release increases the ionic activity product of apatite in the fluid but it can be noted, that only in the case of Ca, SiO_2-based glasses the activity suddenly decreases. This is because the apatite is formed on the surface by consuming the calcium and phosphate from the fluid. This indicates that the surface of CaO, SiO_2-based glasses provide favorable sites for the apatite nucleation. Furthermore, it is possible to observe a silica layer on the CaO, SiO_2-based glasses prior the formation of the apatite in SBF which means that hydrated silica induces the apatite nucleation. This silica layer can be observed on the surfaces of WA glass-ceramics and sintered HA and, as already mentioned, it is not desirable. However, some studies have demonstrated that for β-TCP this silica layer was not formed even after 120 days meaning that the mechanism of precipitation is probably different.

As far as wollastonite-diopside glass-ceramic concerns, it has been hypothesized one mechanism of apatite precipitation that can be summarized in four steps.

1. Dissolution of wollastonite in SBF with release of Ca^{2+} and $HSiO_3^-$ as majority ions, and increase in Ca^{2+}, $HSiO_3^-$, OH^-, ionic activities at the neighbourhood of the reacting surface until they exceed the solubility product of the HA:

   $CaOSiO_3\,(s) + H_2O \rightarrow Ca^{2+}\,(aq.) + HSiO_3^-\,(aq.) + HO^-\,(aq.)$

   With the release of the calcium ions from the wollastonite solid solution, many Si-OH groups are formed in the surface of WD glass-cermic (silica layer). These silanols groups induce heterogeneous nucleation of apatite and the released calcium ions increase the ionic activity product of apatite, enhancing apatite nucleation.

2. Partial dissolution of diopside in SBF with release of Ca^{2+}, Mg^{2+}, and $HSiO_3^-$:

   $CaMg(SiO_3)_2\,(s) + 2H_2O \rightarrow Ca^{2+}\,(aq.) + Mg^{2+}\,(aq.) + 2HSiO_3^-\,(aq.) + 2OH^-\,(aq.)$

3. After that the nucleation of a calcium-deficient hydroxyapatite layer takes place on the porous surface of the material by reaction of SBF phosphate ions with the excess of calcium ions liberated to SBF by the ceramic. The silicate ions liberated by the ceramic can produce a silicon hydroxyapatite.
4. Once apatite nuclei are formed n the surface, they can grow spontaneously by consuming calcium and phosphate ions from the surrounding fluid.

These first four steps do not depend on the presence of tissue, they occur on the material side of the interface. There are, indeed, 6 more steps to reach the real interfacial bonding to bone.

5. Adsoption of moieties (proteins from the blood and tissue fluids from the wound site) in the SiO_2-HCA layer.
6. Action of macrophages, cells derived from circulating white cells, to remove foreign material (i.e. dead tissue, bacteria and other particulates). During this stage the wound is cleaned and new blood vessels begin to enter the nearby tissue.
7. Attachment of mesenchymal cells (adult stamina cells). These are the wound-healing cells and are the first type of cell to interact with the implant.
8. Differentiation of mesenchymal cells into osteoblasts.
9. Generation of extracellular matrix. The osteoblasts produce and lay down collagen fibres in a random fashion.
10. Mineralization of the matrix. Collagen fibres become more organized and mature leading to new bone.

The first four steps are the ones that allow to experiment the bioactivity of the material in the SBF fluid while, to analyze the other 6 steps, *in-vivo* experiments are required.

Chapter 2 : Scaffolds and bone tissue engineering

Tissue Engineering is the field of research using cells and other materials to either enhance or replace biological tissues. It offers vast potential for changing traditional approaches to clinical treatment. And since so many tissues and organs are strong candidates for engineering reconstruction (including bone, cartilage, liver, pancreas, skin, blood vessel, and peripheral nerve) tissue engineering can help meet critical health care needs related to tissue and organ replacement. Tissue engineering systems are also being used as model systems to study cell behavior.

Regenerative medicine is a broad field that includes tissue engineering but also incorporates research on self-healing where the body uses its own systems, sometimes with help of foreign biological material to recreate cells and rebuild tissues and organs. The terms "tissue engineering" and "regenerative medicine" have become largely interchangeable, as the field hopes to focus on cures instead of treatments for complex, often chronic, diseases.

Bone is one of the most common transplanted tissue, the second only after blood. Traditional treatments for large bone defects are based on transplant of autologus bone (from the same patient), allogenic bone (from a human cadaver) or xenogenic bone (from animals). Autologus autografts are considered the best procedures in bone grafting showing properties as osteogenic, osteoiductive and osteoconductive with the best clinical outcomes. The clinical applications are however limited due to their short supply and the high percentage of donor site morbidity. The use of allografts or xenografts could be an alternative for their high availability and low cost. However, these approaches present also risks, like infection transmission and adverse host immune response, resulting in poor outcomes. The limitations of current treatments together with the impact on healthcare system costs encouraged interest in alternative therapeutic solutions. In some situation, moreover, when a critical size bone defect develops, the cells cannot migrate from one side to the other, regeneration is limited, in fact, to a distance of few millimeters creating so a requirement for a solid support (commonly known as scaffold) on which they can anchor and build new bone.

2.1 Scaffolds manufacturing

Most applications involve all these biomaterials as powder or in simple geometries as bloks, pins or splines, but, as it is important to introduce in the body something that can mimic to the best the morphology, structure and function of bone tissue, it has been necessary to develop different structures. With additive manufacturing techniques it has been possible to create three-dimension porous matrices, i.e. scaffolds, and the main advantage of all these technologies is that they allow to manufacture bone grafts with complex shapes as well as designed internal channel networks to mimic bone structures. Anatomical information obtained from patients (by means of magnetic resonance, for example) can be used to design

and optimize the implant for a target defect. Patient-derived cells can be seeded onto the scaffold that works like a template for initial cell attachment and subsequent tissue formation[14].

Basically, in bone tissue engineering, a scaffold provides a proper space in which seeded cells can grow and new tissue can be formed. High porosity is required to offer sufficient space for tissue growth and to increase the volume of the invasion of surrounding tissue. An interconnected pore network is also essential for tissue ingrowth, vascularization and diffusion of nutrients. Pore dimensions in the range of 200 to 350 μm have been found to be ideal for bone tissue in-growth (if the pores are too small, pore occlusion by cell migration can happen) and a porosity more than 70% is beneficial in facilitating cell infiltration, bone ingrowth and internal mineralized bone formation. Yuan et al. found that micropores on the macropore walls of the calcium phosphate ceramic were important in osteoconduction. The degree of porosity, moreover, influences the scaffold mechanical stability, therefore its value should be in the range of strength and stiffness of the host tissue, some scaffolds, for example, were developed with compressive strength of about 5 MPa which is comparable to the compressive strength of cancellous bone.

Some *in-vitro* experiments have been carried out also to prove the biocompatibility of WA-scaffold. It has been demonstrated that MSCs[1] cultured together with the WA scaffolds manufactured by 3D printing proliferated on it with the increase of culture time confirming the non-citotoxic effect of the material. Starting from the positive *in-vitro* results, also the *in-vivo* behavior was tested. A defect on a rabbit mandible was employed for the evaluation of a pure scaffold and a MSCs seeded scaffold, the histological results showed that the scaffold with seeded cells presented a better biocompatibility and enhanced osteogenesis than the pure scaffold, both exhibited good biocompatibility and extensive osteoconductivity with host bone for 8 weeks[15].

So, scaffolds are essential pillars for what bone tissue engineering concerns and after the choice of the appropriate material for one specific application it is important to select the most suitable processing technology to fulfill all the requirements. Polymer foam replication is the most widely exploited technique to produce bioactive glass and glass-ceramic scaffolds. In addition to this method, a variety of different technologies have been developed through the years to produce 3D porous glass and glass-ceramic scaffolds, including sol-gel, organic phase burningout, thermally induced phase separation (TIPS) and freeze casting. Despite the fact that conventional fabrication methods have been widely used over the last three decades to produce promising scaffolds for medical applications, most of the scaffold requirements (*i.e.* pore geometry, pore size, shape and interconnectivity) cannot be fully controlled with many of them. Moreover, depending on the fabrication method used, the 3D scaffold also lacks the mechanical strength necessary to withstand stress and forces of the living tissues (*i.e.* sol-gel method). In addition, some of these processing techniques use organic solvents,

[1] Mesenchymal stem cells, or MSCs, are multipotent stromal cells that can differentiate into a variety of cell types, including: osteoblasts (bone cells), chondrocytes (cartilage cells), myocytes (muscle cells) and adipocytes (fat cells).

and the presence of their toxic residues can cause severe inflammatory response (i.e. TIPS and freeze casting). Furthermore, most of these methods are manual, resulting in poor reproducibility over the large scale and inconsistent outcomes. The table in the following page (Table 2-1) briefly describes the main features of each method.

2.2 Additive manufacturing

The emerging need for innovative 3D constructs with tailored physicochemical and mechanical features has led to the development of new manufacturing technologies. The use of additive manufacturing (AM), or also called solid free form fabrication (SFF), rapid prototyping (RP) or more recently 3D printing processes, to produce custom-made devices with well-designed architecture, has become a fast-developing research field in the last few years. AM is defined as "the process of joining materials to make objects from three-dimensional model data usually layer upon layer". Differently from the other technologies that remove material from a bulk, using AM techniques 3D objects are built through a layer-by-layer approach *via* the processing of solid filament, liquid or powder stock materials. AM provides exclusive methods to produce accurate (macro-architecture as well as microstructure) and consistent (mechanical properties, porosity and interconnectivity) bone-like substitutes matching patient's defects.

Medical images of the anatomic site are acquired by computer tomography (CT) or magnetic resonance imaging (MRI). The 2D image data are then treated by computer-aided design (CAD) software, and afterward the obtained 3D model is converted into a standard tessellation language (STL) file. Subsequently the "*.stl"* file is sliced into layers and loaded in the AM machine. Some devices, however, don't need this slicing process.

According to the fabrication process, the 3D build parts can need further finishing and cleaning work. At present, different AM techniques have been widely explored for TE scaffold fabrication, although none of those cited has been acknowledged as a gold standard approach.

Here there is a brief overview of the most important additive manufacturing technologies.

2.2.1 Stereolitography

Stereolithography (SLA) is the oldest AM technology. It uses ultraviolet (UV) light or laser to polymerise layer-by-layer a photosensitive polymer. Once one layer is completed, the construction platform is vertically lowered to a given distance and a new uniform layer of resin is placed on the top of the previous solidified one. The process is repeated until the 3D object is completed. Further actions include the removal of non-polymerised resin and the post-curing of the printed 3D part under UV light. However, considerable shortcomings (for example the shrinkage of the structure during the production process, the necessity of a support and the presence of a toxic resin) limit the use of this technique.

Table 2-1: Main features of organic phase burning out, foam replication, sol-gel, thermally induced phase separation (TIPS) and freeze casting methods

Method	Description	Advantages	Disadvantages
Organic phase burning out	A blend is obtained by mixing particles and organic phase, after they are treated to remove the organic phase and sinter the glass.	- No organic solvent	- Residuals of porogens. - Low porosity and limited interconnectivity.
Foam replication	Impregnation of a polymeric sponge template in a glass-based slurry followed by a thermal treatment to remove the organic phase and sinter the glass.	- No organic solvent - Control of porosity and pore size	- Possibility of inhomogeneous coating of the foam. - Low mechanical strength.
Sol-gel	A solution of metal alkoxides leads to the formation of the sol phase, made by solid particles that then will condense in gel-like materials. After a drying process the so obtained material s treated at high temperature	- Hierarchical pore structure - Interconnected macropores - Nanoporous texture	- Many variables affect the final morophology (glass phase, surfactant, gelation time). - Low mechanical strength.
Thermally induced phase separation (TIPS)	A polymer mixed with/without glass particles is dissolved in a solvent and a liquid-liquid or solid-liquid phase separation is obtained by lowering the temperature. The solvent is removed by sublimation to give a porous structure.	- Incorporation of biologically active molecules - High porosity	- Slight changes in the parameters affect the morphology of the scaffold. - Possibility of solvent residues.
Freeze casting	The method involves the rapid freezing of colloidally-stable suspension of particles in a nonporous mold. The frozen solvent is removed by sublimation to avoid cracking prior to sintering.	- Oriented microstructure - High mechanical strength in the direction of orientation	- Small pore size. - Possibility of solvent residuals.

2.2.2 Selected laser sintering

Selected laser sintering (SLS) process is based on the use of a high intensity laser beam such as CO2 that selectively sinters regions of powder-based material placed in a powder bed until the formation of a powder layer. After the generation of the first layer, the powder bed is vertically lowered by one layer thickness and the new layer of powder is spread mechanically by a roller on the top of the previous one. In this technology, the non-sintered powder serves as support for the build-up of the next layers. There are two types of SLS: the direct and the indirect one. In direct SLS powders are just melted and consolidated by the laser, in indirect SLS, only a binder material is melted by the laser to bond powders creating what is known as "green part", in both cases further heat treatments are required to sinter the powders and consolidate the structure. Usually, TE scaffolds produced *via* SLS technique show low mechanical properties, however, using a SLS method, it has been possible to fabricate an apatite-mullite glass-ceramic with good surface finish and mechanical properties in the range of cancellous bone.

Recently 3D porous AW scaffolds with different level of porosity and good mechanical properties (close to those of natural bone[16])have been realized with this technique.

2.2.3 Fused deposition modeling

Fused deposition modeling (FDM) is based on the melting and extrusion of material (usually a thermoplastic polymer) onto a platform. The filament of material is provided by two rotating rollers to a mobile nozzle, which moves in *x* and *y* direction. Through an orifice in the extruder head the material can be deposited on a platform. After fabrication of the first layer and when the material is solidified, the platform moves downwards in *z*-direction and the process is repeated layer-by-layer until the 3D object is completed. The use of FDM technique allows the manufacture of interconnected porous scaffolds with an extremely reproducible architecture, with no need of solvents, and at a quite low maintenance cost. However, this strategy has two main disadvantages: one is the use of material in the form of filament with fixed diameters and the other is the potential negative effect of high temperatures on the raw materials.

2.2.4 Powder-based 3D printing

Some scaffolds were realized with 3D printing during this study in order to verify the maintenance of the shape for each heat treatment.

Three-dimensional printing (3DP) is an ink-jet printing technology, developed at MIT (Cambridge, MA) in 1989. It is used to produce complex 3D solid objects by jetting a liquid-based binder onto a bed of loose powder. 3DP technology has been largely used to create 3D tissue substitutes from a wide range of materials. Figure 2-1 shows the basic components of the 3D printer. On the left side of the figure there is the feeding system, the left piston moves up at every layer and the roller spreads the new layer on the right side, the right piston moves

down each time that the left one moves up and the part is so constructed on the right side. What is missing in the image is the printhead, the device placed over this set that delivers selectively the binder on the powderbed.

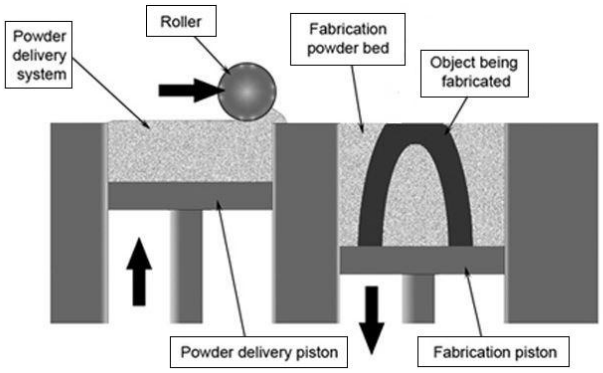

Figure 2-1: Schematic setting of a powder based 3D printer.

For the manufacture of medical devices the main advantages of this technology derive from the possibility to fabricate 3D custom substitutes with defined design, controlled and interconnected porosity, with a wide range of materials, and also without the contamination problems related to the use of toxic solvents.

However, process parameter optimization, appropriate binder selection, and depowdering (*i.e.* removal of the loose powder) after printing are important features to be considered for the final success of the printed parts and, furthermore, good handling skills are required from the operator. Moreover, before starting the process, and after the material selection, thorough optimization of the printing parameters, *e.g*. layer thickness, powder packing density, powder wettability, powder flowability as well as binder drop volume, is necessary to obtain a good outcome.

For any new powder-based material the optimization process may require a long time; this can be considered one of the major shortcomings of 3DP technique.

Liquid binders are the most versatile methods as they work with almost any material. However, in the case of organic binders, they can dry in the printhead, causing the obstruction of the nozzle. The use of an in-bed binder is an alternative method: a powder-based component is added to the starting formulation and it binds the particles after interaction with a sprayed liquid. Even though, it is a time-consuming process, as it requires the further step of mixing two materials any time a new powder is processed, it reaches higher green body strengths if compared to liquid binders. Subsequently, a heat treatment needs to be performed on the green bodies to burn out the binder and any additive used, and consolidate the structure. *Sintering* is the most important post-processing step, which provides an increased mechanical strength to the 3D printed object. Every material has specific sintering temperature, usually defined as the temperature where the maximal densification rate is being reached. In the present work glass-ceramics have been treated so it was of great importance not only the sintering temperature but also the crystallization one.

During the sintering/crystallization processes the composition (*i.e.* phase changes), mechanical and structural properties of a material are also influenced.

In most cases, heat treatment allows a structure to retain its shape, even though the process can cause a significant degree of sample shrinkage. This phenomenon can be compensated by scaling the initial CAD model according to a pre-determined correction factor.

Because of all these influencing factors on the final part, the aim of all the first experiments was to identify all the suitable printing parameters.

Chapter 3 : Methods and materials

3.1 Materials

The material analyzed in the present work is a WD glass-ceramic. It has been produced in two different composition, the eutectic compsition and another one in which a sodium-phosphate flux has been added. The aim of this second composition was to verify if the flux could help the crystallization process. As a matter f fact this kind of flux produces a liquid phase that promotes crystallization of the desired phases during the ceramization process and the formation of a glassy phase during the following cooling.

In order to check if the behavior of the WD glass-ceramic during the SBF test (*i.e.* the formation of the apatite-like layer on the surface)was correct, the material has been compared with WA glass-ceramic, that was used therefore, as standard material. In the following table the nominal compositions of the three materials are quoted.

Table 3-1:Nominal composition of the three glass.cermics

Theoretical compositions %wt	SiO_2	CaO	MgO	P_2O_5	CaF_2	Na_2O
W-A	34.0	44.7	4.6	16.2	0.5	-
W-D eutectic	53.985	34.847	11.168	-	-	-
W-D with flux	51.58	32.1	11.5	2.5	-	2.2

The glasses were obtained with the traditional melting-quenching technique. The WD eutectic parent glass was melted in a furnace at 1600 °C for 1 hour, WD with the flux was melted at 1380°C for 1h while WA glass ceramic was melted in the furnace at 1500°C for 1 hour following Kokubo's protocol[2]. Frits were obtained by quenching the glass in water and then milled with a fast planetary ball mill with sintered yttria stabilized zirconia balls.

Milled powders were then sieved to obtain different particle size distributions. For WD glass-ceramic 3 different size distributions were obtained (45-100 μm, 25-45 μm and <25μm) and only one for the WA glass-ceramic (45-100 μm). Three different particle size distributions were needed for WD glass-ceramic in order to verify the behavior with different heat treatment. Since the crystallization starts from the surface it was expected to be promoted in case of small particle size.

3.2 Specimens preparation

First of all, pressed tablets were prepared using 0.9 g. of powder and with a force of 15 kN applied for 30 seconds. The diameter of all the tablets was 16 mm and the thickness have been measured for each sample by means of a caliber. Both dimensions were measured also after each heat treatment to quantify the shrinkage.

Other tablets were prepared also by 3D printing and in this case, all the dimensions were taken before and after the heat treatment. The initial dimensions were, indeed, influenced by the handling after printing and by the support removing operations. When the parts are depowered from the printer they have a support structure on the basis that is essential for the success of the print-job but it must be removed before further operations. Some scaffolds were also printed to check the behavior during the heat treatments. The three-dimensional image of tablets and a scaffold are showed below (Figure 3-1).

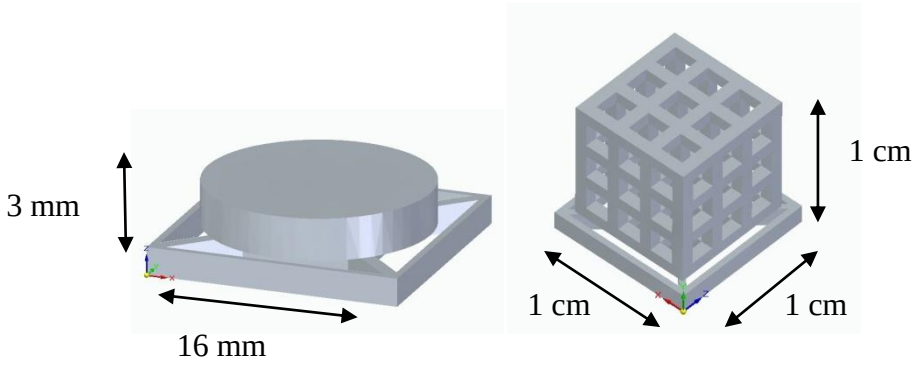

Figure 3-1: 3D Image of printed tablet and scaffold with support.

It was opossible to print tablets and scaffolds only with the size distribution of 45-100 μm because it was the only one that showed the suitable flowability.

Indeed, it is of great importance in 3D printing that the granular raw material has the correct flowability to obtain a smooth and homogeneous powder bed surface. Too low values of flowability, in fact, decrease fabrication resolution due to insufficient recoating and on the other hand, very high flowabilities do not provide sufficient powder bed stability for 3DP.

Housner ratio (R) is the number correlated to the flowability and it is calculated by the following formula:

$$R = \frac{\rho_T}{\rho_B} \quad (1)$$

where ρ_B is the bulk density and ρ_T is the density of the tapped bulk. R is not an absolute property of the material but it depends on the method used to determine it. It can be observed that with increasing values of this ratio (*i.e.*:decreasing powders size), the flowability decreases and a value of the R higher than 1.25 indicates poor flowability.

The first investigations (DTA,HSM and density) were carried out for pressed tablets of every particle size distribution but mechanichal, degradation and bioactivity tests have been done only for pressed and printed tablets realized with the biggest particles in order to obtain coherent and easily comparable results.

3.3 DTA analysis

Differential thermal analysis (DTA) has been carried out in order to investigate phase transformation occurring during the heating of the material. This test is useful in particular to determine the crystallization temperature of the material in order to identify the more appropriate heat treatment to obtain required phases.

In DTA, the material under study and an inert reference are made to undergo identical thermal cycles while any temperature difference between sample and reference are recorded. This differential temperature is then plotted against time, either against temperature to obtain DTA curve or thermogram respectively. Changes in the sample, either exothermic or endothermic, can be detected relatively to the inert reference. In this study, DTA were performed for each material and for the biggest and the smallest size distribution on order to check if smaller particles effectively crystallized more easily than the bigger ones.

3.4 Hot stage microscopy

The sintering ability of the novel glass powders was determined by using hot stage microscopy (HSM). This device, makes it possible to observe and record the changes of samples contours with temperature. In particular, in the manufacture of glasses and ceramics HSM is used to study the characteristic temperatures of softening, melting, flowing and sintering. One method has also been developed to precise measuring of the coefficient of thermal expansion of some materials [17]. HSM, moreover, allows to establish sintering curves of the material. This curve presents the dependence between the growing temperature and the ratio (expressed in%) of two samples: the initial sample (prior to heating) and the one at a given temperature of its expansion or shrinkage.

The analysis has been carried out for both materials and for each particle size distribution as for the DTA procedure.

3.5 Heat treatments and shrinkage evaluation

Three heat treatments have been done for each material in order to identify the best combination of degree of crystallization and shape maintenance. The rate of heating and dwelling time were decided on the basis of previous works carried out on WD glass-ceramic[18] and the different temperatures based on DTA results. The table below shows all the treatments that were done on printed tablets and scaffolds with particle size of 45-100 μm and on pressed tablets for every particle size distribution.

Table 3-2: Heat treatments for the WD glass-ceramics

	Heating rate	T1	T2	T3	Cooling rate	Tf
WD + flux	5°/min	775°C	800°C	825°C	10°/min	RT
WD eutec.	5°/min	800°C	900°C	1100°C	10°/min	RT

For all the tablets (printed and pressed) the axial (Δs), radial (Δd) and the volumetric (ΔV) shrinkage have been calculated with the following formulas:

$$\Delta s\% = \frac{s1 - s2}{s1} \quad (2)$$

$$\Delta d\% = \frac{d1 - d2}{d1} \quad (3)$$

$$\Delta V\% = \frac{V1 - V2}{V1} \quad (4)$$

where numbers 1 and 2 are referred to initial and final state respectively.

As far as WA glass-ceramic is concerned, the correct heat treatment to obtain the two crystalline phases consists on a heating rate of 1°C/min until 1050°C followed by a dwelling time of 4 hours.

3.6 Density and porosity measurements

3.6.1 Archimede's method

Apparent porosity of samples was determined by Archmedes´s principle according to ISO 18754, "Fine ceramics (advanced technical ceramics). Determination of density and porosity measurements"[19]. Dry weight (W1) was measured by an high precision balance (Mewes & Götzl Wagetechnik, DE). The specimens were then submerged in distilled water, placed in a vacuum chamber for 30 minutes. The vacuum method is preferable to the one that involves 3 hours of boiling for materials that could be reactive with water as in this way the contact between the material and water is reduced at minimum. Then, the specimens were taken out and dried with a wet tissue in order to remove only the excess water and the soaked weight was measured (W3). After that the weight of specimens suspended in water was measured (W2).

The apparent porosity (P_a) was calculated by the following equation:

$$P_a\ (\%) = \left(\frac{W3 - W1}{W3 - W2}\right) \times 100 \quad (5)$$

Apparent solid density ($\rho_{app.}$) and bulk density (ρ_{bulk}) have been furthermore calculated with the following equations:

$$\rho_{app.} = \left(\frac{W1}{W1 - W2}\right) \times \rho 1 \quad (6)$$

$$\rho_{bulk} = \left(\frac{W1}{W3 - W2}\right) \times \rho 1 \quad (7)$$

Where $\rho 1$ is the density of distilled water at 25°C.

ρ_{app} corresponds to the ratio of the mass of the dry material to its apparent solid volume (the apparent solid volume is the sum of the respective volumes of the solid material and the closed pores).

ρ_{bulk} corresponds to the ratio of the mass of the dry material to its bulk volume (the bulk volume is the sum of the respective volumes of the solid material the open pores and the closed pores).

The average of three specimens for each composition was considered.

3.6.2 Pycnometer measurements

With the method described above it is not possible to determine the total porosity of the samples. It is possible, instead, to calculate the total porosity (P_{tot}) with the following formula:

$$P_{tot}\ (\%) = \left(1 - \frac{\rho_{bulk}}{\rho_{real}}\right) \times 100 \quad (8)$$

in which the real density ρ_{real} and ρ_{bulk} are required (calculated by the Archimede's method).

True density of a glass-ceramic, that is the density of the pore-free material, can be calculated from the molecular weight and crystalline lattice which is determined by X-ray diffraction, but this procedure is not a routine technique. Currently, the device considered to give the most reliable results to the true density is the helium pycnometer[2]. Helium is used to determine the volume of the sample and the efficacy of the procedure is based on the fact that helium can penetrate into smallest pores permitting to approach the real volume. Knowin then both the real volume and the weight of the sample, the real density can be directly calculated.

The volume is measured by filling the sample cell with helium to the required filling pressure, then the gas expands in the expansion cell and the final pressure at the equilibrium is recorded. The real volume (V_{sample}) is then calculated as:

[2] Viana *et al.* demonstrated that this technique has a good reliability and that the variation in pycnometric density due to operating parameters can affect the accuracy of the result to the nearest 0.01 g/cm^3.[20,21]

$$V_{sample} = V_{sample\ cell} - \left(\frac{V_{exp.cell}}{\frac{P_r}{P_f}} - 1 \right) \quad (9)$$

where P_r is the run fill pressure is and P_f is the final one. $V_{sample\ cell}$ and $V_{exp.cell}$ are determined by calibration.

3.7 X-Ray diffraction

X-ray diffraction (XRD) analysis was performed to investigate the presence of crystalline phases in the novel materials. It has been done for materials after the established heat treatment. The treated tablets were milled in order to obtain particle size < 45 μm.

XRD is based on constructive interference of monochromatic X-rays and a crystalline sample. These X-rays are generated by a cathode ray tube, filtered to produce monochromatic radiation, collimated to concentrate, and directed toward the sample. The interaction of the incident rays with the sample (Figure 3-2) produces constructive interference (and a diffracted ray) when conditions satisfy Bragg's Law:

$$n\lambda = 2d \sin\theta \quad (10)$$

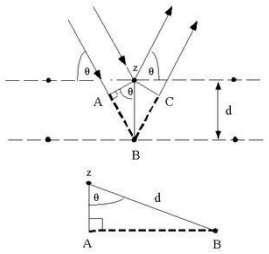

Figure 3-2: Scheme of constructive interference in XRD

This law relates the wavelength of electromagnetic radiation (λ) to the diffraction angle (θ) and the lattice spacing in a crystalline sample (d). These diffracted X-rays are then detected, processed and counted. By scanning the sample through a range of 2θ angles, all possible diffraction directions of the lattice are supposed to be attained due to the random orientation of the powdered material. Conversion of the diffraction peaks to *d* allows identification of the mineral because each lattice has a set of unique *d*-spacings. Typically, this is achieved by comparison of *d*-spacing with standard reference patterns.

3.8 Mechanical characterization

Mechanical tests of ceramics and brittle materials in general are, in most cases, performed in bending, where an uni-axial stress state occurs. This technique has some advantages such as the easy testing procedure and the simple specimen preparation. But, as most commercial

produced components are bi-axially loaded, many proposal for bi-axial strength testing have also been made. This stress state is more searching for defects than the uni-axial one. Bi-axial tests are often used in an axisymmetrical testing assembly where the disc is supported by a ring and loaded from the opposite site by another, smaller concentric ring (ring on ring test). In the area underneath the smaller ring exists an equi-biaxial stress state where the fracture is expected to start. Other bi-axial tests are for example the ball-on-ring test and the ball-on-ring of balls test. For all these methods, a more o less perfect flat disc is required and often polishing of the surface is necessary as any deviation from flatness lead to additional stresses and results become hardly interpretable. Some other procedures which tolerate a small out of flatness of the disc have been developed.

3.8.1 Ball on three balls test

One of these bi-axial method is the ball-on-three-balls (B3B) test, in this case the specimen is supported on three ball and loaded symmetrically by a fourth ball. (

Figure 3-3). This is the most tolerant test to some out-of-flatness of the specimen and also for small geometries or some misalignment. This test is, furthermore, suitable for as-sintered and very small specimens as it is recognized that friction is much smaller than in the commonly used bending test.

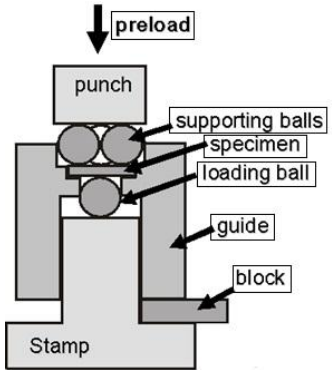

Figure 3-3: Scheme of the B3B test set up.

The maximum principal stress in the disc, which occurs on the disc surface opposite the centered loading ball (where the stress state is purely biaxial), is used to define the strength. To reduce the parameters having influence on this stress, all the balls have the same size and the three supporting ones are in touch with each other, the three point of contact with the specimen, moreover, form an equilateral triangle; its circumradius is called support radius of the disc; R_a. Tensile stresses also occur around the loading areas, caused by loading and supporting balls. They are higher than the smaller the radius of the balls, limiting the minimum size of them.

The stress field (Figure 3-4) in the specimen depends on various factors such as the applied force, the disk thickness and diameter, the size and position of the balls and also on the elastic properties of both materials (disc and balls). This dependence on so many factors is the most important disadvantage for this procedure and different approaches have been made for the

analytical calculation of the stress distribution in centrally loaded biaxial disc tests. It has been performed, however, an FE (finite element) analysis that showed some very important simplifications.[22]. By means of this analysis it has been shown, for example, that the stress field in the disc does not depend on the elastic constants of the balls, it does not depend, also, on the Young's modulus of the tested material but it depends on its Poisson's ratio. These conclusions suggested that the stress field in the disc does not depend on the non-linear changes in the loading geometry which are primarily caused by the deformation of the balls. It could also be shown that the loading situation can be approximated by a simple point loading mode.

On the basis of this FE- analysis the maximum stress (σ_{max}) can be calculated by the following formula:

$$\sigma_{max} = f * \frac{F}{t^2} \qquad (11)$$

Where F is the applied force, t is the thickness of the disc and f is a dimensionless factor that depends on the ratio of the thickness to the radius of the disc, ratio of support radius to the disc radius (R_a) and Poisson's ratio of the tested material.

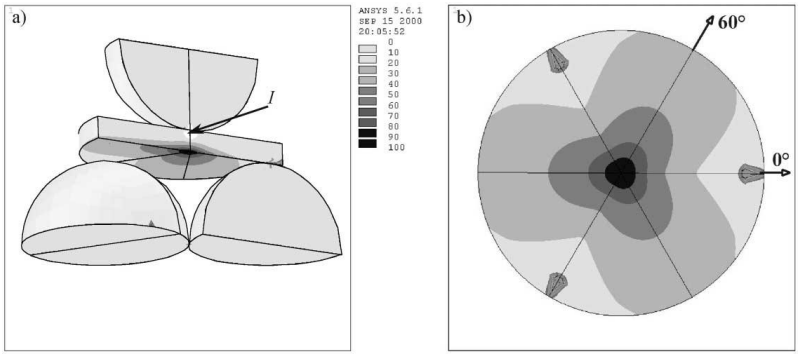

Figure 3-4: Example of a stress field in a disc for a typical loading condition in B3B test. The white areas indicated with an arrow stand for compressive stresses (contact area between support balls and the disc).

Specimens were tested in a universal testing machine (Z005, Zwich, Ulm, Germany), a preload of 20KN was applied before the positioning aid was removed which allowed the supporting balls to roll free upon fracture of the specimen. Tests were conducted at a 0,02mm/sec speed.

The strength data obtained using the B3B test was analyzed using Weibull statistic.

3.8.2 Weibull statistic

That of Weibull is one of the statistics most used to describe the strength distribution of ceramics and brittle materials, in general. It is considered the backbone in the mechanical design process of ceramics components.

With metals, for example, it is possible to determine the maximum stress that will be present in the component and from that the right material is chosen. This approach is referred to a deterministic analysis and it does nott work with ceramics and brittle materials because of the large scatter of values from the experimental procedure. Weibull's is a probabilities approach in which the scatter is represented as in a quantitative way in order to allow these materials to be used safely.

The theory is based on the weakest link hypothesis, i.e. the specimen fails if its weakest volume element fails. The analysis consists of converting a set of rupture stresses into an experimental probability distribution.

The distribution function contains three parameters but for ceramics the simplified form with two parameters is usually adopted as it seems to reflect the observed behavior better.[23] The probability of survival is expressed as follows:

$$P_s = \exp[-\left(\frac{\sigma}{\sigma_0}\right)^m] \quad (12)$$

Where the two parameters are: m (Weibull modulus) and σ_0 (characteristic strength for which the survival probability is 0.37%). Weibull modulus describes the variability of the measured values, the higher is its value the lower is the variability of the strength and values for ceramics are generally in the range 5-15.

To manipulate data from the experiments, P_s is calculated by an estimator expressed as follows:

$$P_s = \frac{x - 0.3}{N + 0.4} \quad (13)$$

Where x is the number of the sample considered and N is the total number of the samples. In order to perform a good analysis the number N should not be lower than 30 [24] .

Taking the logarithms of both sides of the equation (12) twice results:

$$\ln\left[\ln\left(\frac{1}{P_s}\right)\right] = m\ln\left(\frac{\sigma}{\sigma_0}\right)^m = m\ln\sigma - m\ln\sigma_0 \quad (14)$$

Plotting then $\ln\left[\ln\left(\frac{1}{P_s}\right)\right]$ versus $\ln\sigma$ typically results in a straight line with the slope *m* and from the intercept *n* with the *Y* axes it is possible to calculate the value of σ_0 as: $e^{(-\frac{n}{m})}$.

Determination of *m* and σ_0 is in this way in obtained by linearization of (14) equation and performance of linear regression on data.

3.9 Degradation tests

3.9.1 TRIS preparation

Degradation test was performed according to ISO 10993-14 "Biological evaluation of medical device- Part 14: Identification and quantification of degradation product from ceramics"[25].

Tests were carried out in Tris[hydroxymethyl]aminomethane - HCl solution (pH 7.4) using triplicate samples. Tablets were submerged in a specific amount of TRIS in plastic bottles and placed in incubator at the temperature of 37°C. The amount of TRIS per tablet was calculated on the basis of the sample weight respecting the ratio: 1g/20ml.

3.9.2 Ion concentrations measurements

Measures were taken every week for 8 weeks. The amounts of ions dissolved from the glasses in TRIS buffer solution ($Ca^{2+,}$ Na^{2+}, Mg^{+}, K^{+}, PO_4^{3-}, Si^{4+}) were evaluated by inductively coupled plasma (ICP). After each period of time, to prepare the samples for ICP, the solution was moved from the plastic container to a glass flask and diluted with distilled water until the volume of 50 ml. As the same tablets have been used for all the different periods of time, it was of great importance to rinse carefully all of them during this procedure at the end of every period. After that, the samples were again submerged in new TRIS solution.

In addition to the samples to be measured, 4 standard samples were required for calibration, one standard test solution and also one standard HA solution.

The table below (Table 3-3) shows the components and the amount of each solution prepared.

Standard solutions from 0 to 3 are made for calibration of ICP device. Standard test and standard HA are solutions with known compositions that allow to check the correct running of the device during the measurements, they are of essential importance as the entire procedure takes typically more than 2 hours and the make it possible to identify eventual errors and to stop the procedure if it is necessary. Ions as Ca^{2+}, Mg^{2+}, K^{+}, Na^{+}, PO_4^{3-} and Si^{4+} were available from other standard solutions with concentration of 1mg/ml. The amounts in the table are referred to these solutions.

Internal Standards (IS) for Ytterbium and Lithium are specific solutions aimed to improve both the accuracy and precision of the analytical results. They compensate for a variety of factors that can degrade the analytical performance including instrument drift or sample matrix effect and the intensity readings for all elements are corrected.

Table 3-3:Components and amounts of calibration solutions, test solutions and measured samples for degradation tests. The values highlighted are referred to solutions with a concentration of 10mg/l, HA is a solution made of HA powder and e-pure water.

	Standard0	Standard1	Standard2	Standard3	Standard test	Standard HA	Samples for measurement
Ca^{2+}	-	50µl	500µl	1500µl	500µl	-	-
Mg^{2+}	-	50µl	250µl	500µl	500µl	-	-
K^{+}	-	50µl	250µl	500µl	500µl	-	-
Na^{+}	-	250µl	250µl	500µl	500µl	-	-
PO_4^{3-}	-	50µl	250µl	500µl	500µl	-	-
Si^{4+}	-	50µl	500µl	100µl	250µl	-	-
IS Yb	0,5ml	0,5ml	0,5ml	0,5ml	0,5ml	0,5ml	0,1ml
IS Li	0,5ml	0,5ml	0,5ml	0,5ml	0,5ml	0,5ml	0,1ml
HA	-	-	-	-	-	0,5 ml	-
HCl-15%	2ml	2ml	2ml	2ml	2ml	0,5ml	-
H2O e-pure	Left until 50ml	Left until 50ml	Left until 50ml	Left until 50ml	Left until 50ml	Left until 50ml	4,4ml
TRIS	10,5ml	10,5ml	10,5ml	10,5ml	10,5ml	2,1ml	-
Aliquot	-	-	-	-	-	-	5ml

3.10 Bioactivity investigations

3.10.1 SBF preparation

SBF solution was prepared according to Kokubo's protocol. Table 3-4 shows the ion concentration of SBF compared to the one of blood plasma [26] and Figure 3-5shows the equipment set-up.

All the chemical reagents have been stocked in a dessicator before utilization. Ion-exchanged and distilled water were used. Since SFB is supersaturated with respect to apatite, precipitation was quite easy and appropriate carefulness has been required: all chemicals were introduced in small amounts bit by bit and before dissolving one reagent the previous one had to be completely dissolved. It has been necessary, also, to check that the preparing solution

was always kept colorless and transparent and that no deposit occurred on the surface of the bottle. In that case preparation of solution should have been abandoned.

Table 3-4:Ion concentration in SBF compared with ion concentration in human blood plasma

Ion	SBF	Blood plasma
Na^+	142,0	142,0
K^+	5,0	5,0
Mg^{2+}	1,5	1,5
Ca^{2+}	2,5	2,5
Cl^-	147,8	103,0
HCO^-	4,2	27,0
HPO_4^{2-}	1,0	1,0
SO_4^{2-}	0,5	0,5
pH	7,40	7,2-7,4

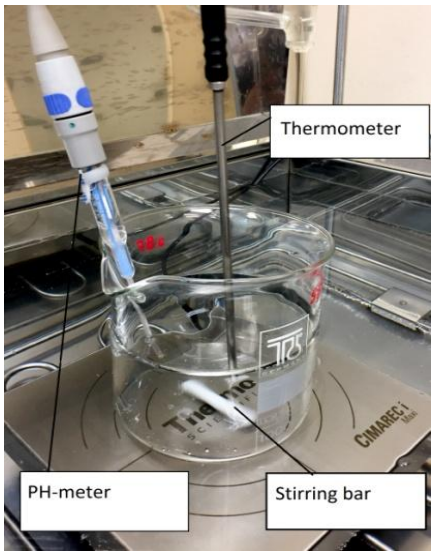

Figure 3-5: Equipment for preparing SBF

In order to prepare 1000 ml of solution, first of all, 700 ml of ion-exchanged and distilled water were put into a beaker with a stirring bar and heated up to 36,5 ±1,5 °C. Then, the reagents were added following the order and in the amounts showed in Table 3-5. It has been of essential importance not to dissolve several reagents simultaneously but to do it only when the previous one was completely dissolved. Moreover, large amounts of TRIS could not be added at a time because the radical increase in local pH of the solution could lead to the precipitation of calcium phosphate.

The solution was ready when the pH was exactly adjusted at the value of 7.40 and the temperature at 36.5°C on condition that the rate of solution temperature increase or decrease was less that 0,1°/min.

Table 3-5:Order, amounts and purity of reagents for preparing SBF.

Order	Reagent	Amount	Purity %
1	NaCl	8,035 g	99,5
2	$NaHCO_3$	0,355 g	99,5
3	KCl	0,225 g	99,5
4	K_2HPO_4	0,176 g	99,0
5	$MgCl_2*6H_2O$	0,311 g	98,0
6	1,0M- HCl	39 ml	-
7	$CaCl_2$	0,292 g	95,0
8	Na_2SO_4	0,072 g	99,0
9	TRIS	6,118 g	99,0
10	1,0M-HCl	0-5 ml	-

The pH- adjusted solution was then poured from the beaker to a 1000ml volumetric flask, the surface of the beaker was rinsed with ion-exchanged and distilled water. The flask was kept in the water to cool it down to 20°C and after that distilled water was added up to the marked line. In order to preserve SBF, it was put in a plastic bottle with a lid and kept at 5-10°C.

For each specimen, the volume of SBF needed for testing was calculated on the basis of the following formula:

$$V_{SBF} = \frac{S_a}{10} \quad (15)$$

Where V_{SBF} is the volume of solution needed (ml) and S_a is the apparent surface area of specimens (mm^2). The apparent surface area was calculated by means of a caliber: the axial and radial dimensions were measured and the area calculated taking in account the two basis and the lateral surface of the tablet.

Specimens could have been placed in two different ways, showed in fig. 3-6, as fo this work concern they were placed in the second way and it has been essential to examine apatite formation for the lower surface as it is possible that apatite precipitate homogenously in SBF and can deposit on the upper surface failing the analysis.

The specimens were incubated at a constant temperature of 37,0°C, different from Kokubo's protocol that suggested 36,5°C, for each different time period (1,2,3 and 4 weeks) without refreshing of solution.

Ion leaching was evaluated and furthermore, structural characteristic and chemical composition were investigated by means of a SEM/EDX system.

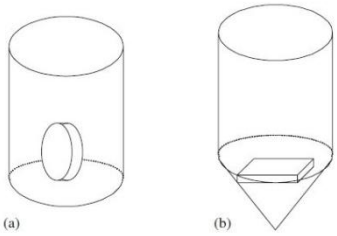

Figure 3-6: Position of specimens in SBF.

3.10.2 Ion concentrations analysis

ICP device has been used to analyze ion leaching for both TRIS and SBF tests.

Table 3-6:Components and amount of calibration solutions, test solutions and measured samples for bioactivity test. The values highlited are referred to solution with a concentration of 10 mg/l, HA is a solution made of HA powder and e-pure water. TRIS solution in this case is different from the one previously described and is obtained withut HCl

	Standard0	Standard1	Standard2	Standard3	Standard test	Standard HA	Samples for measurement
$Ca2^+$	-	50µl	500µl	500µl	1000µl	-	-
$Mg2^+$	-	50µl	250µl	100µl	250µl	-	-
K^+	-	50µl	500µl	1000µl	2000µl	-	-
Na^+	-	50µl	500µl	1000µl	2000µl	-	-
PO_4^{3-}	-	50µl	500µl	1000µl	2000µl	-	-
SO_2	-	50µl	250µl	1000µl	2500µl		
Si^{4+}	-	50µl	500µl	100µl	2500µl	-	-
IS Yb	0,1ml	0,5ml	0,5ml	0,5ml	0,5ml	0,1ml	0,1ml
IS Li	0,1ml	0,5ml	0,5ml	0,5ml	0,5ml	0,1ml	0,1ml
HA	-	-	-	-	-	0,5 ml	-
HCl-15%	0,08ml	0,4ml	0,4ml	0,4ml	0,4ml	0,08ml	-
H2O e-pure	Left until 10ml	Left until 50ml	Left until 50ml	Left until 50ml	Left until 50ml	Left until 10ml	-
TRIS	0,2ml	1ml	1ml	1ml	1ml	0,2ml	-
Aliquot	-	-	-	-	-	-	9,8ml

Preparation of specimens began by moving 5 ml of solution from the incubator to a 25ml flask and diluting with e-pure water, from this solution aliquots were then collected. Tablets

that were immersed were then removed, carefully rinsed with e-pure water and placed in a dessicator for natural drying, no heating was performed. Both in TRIS analysis and in this case some standard solutions have been prepared to calibrate ICP device. The table above (Table 3-6) shows the compositions of these solutions.

3.10.3 SEM surface characterization

Morphology of the tablets' surface was analyzed by means of a scanning electron microscopy. This device comprises of an electron generating component called the gun, a column through which the electron beam travels, a series of lenses to shape the electron beam, the sample chamber at the base, and a series of pumps to keep the system under vacuum. The image of the analyzed surface is formed by secondary electrons that are low energy electrons formed by inelastic scattering. The major influence on SE signal-generation is the shape (topography) of the specimen surface. Secondary electrons provide particularly good edge detail. Edges look brighter than the rest of the image because they produce more electrons. To avoid the formation of electrostatic charge on the sample it had to be made conductive by a layer on its surface.

The SEM was coupled with an EDX equipment to accomplish a qualitative estimation of the surface composition.

Chapter 4 : Results and discussion

4.1 XRF and DTA results

The obtained glass powders were subjected to XRF analysis to verify the correct compositions. Some differences were observed from the theoretical compositions due to the production process. Indeed, contamination with miller materials and evaporation of volatile components are possible. The following table (Table 4-1) shows the results.

Table 4-1: XRF results on parent glasses.

Real composition %wt	SiO_2	CaO	MgO	P_2O_5	CaF_2	Na_2O
W-D eutectic	54.47	34.42	11.1	-	-	-
W-D with flux	51.4	32.9	11.2	1.98	-	2.36

The second analysis carried out on the WD parent glasses powders was the DTA. Heat treatments of glasses induce sintering but in some cases the concomitant process of crystallization occurs. From DTA analysis it is possible to understand if this crystallization process takes place as the traces should show exothermic peaks. The following image (Figure 4-1) shows the traces for both materials.

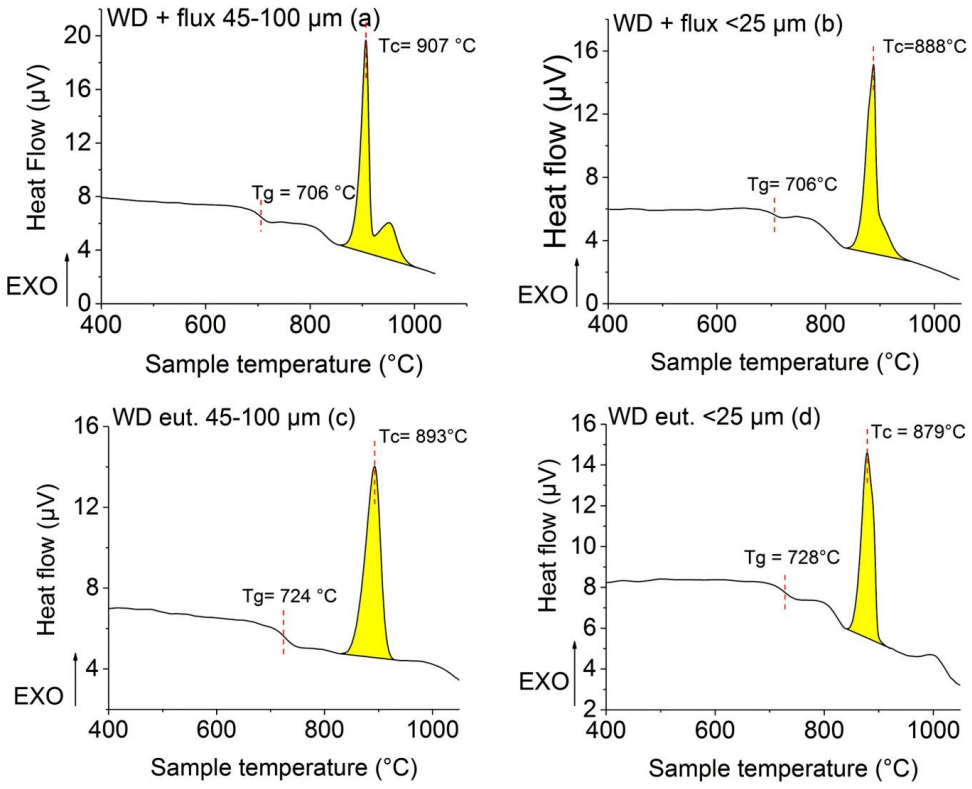

Figure 4-1: DTA traces for WD + flux and WD eutectic, 45-100µm (a,c), <25µm (b,d).

All plots show a noticeable exothermic peak corresponding to the crystallization process of the glass-ceramics. It is clear from this image that, for both materials, the smaller particle size is associated with a lower crystallization temperature. In the case of WD + flux the difference between the two temperatures is even higher than for the eutectic composition. This evidence leads to think about a peculiar mechanism of crystallization known as surface crystallization. This kind of phase transformation is a thermally induced process for particles with higher surface area. Therefore, considering powders under the same heating rate, for the smaller ones the phase transformation starts at lower temperatures. It has been demonstrated in other works that in the case of surface crystallization, a smaller particle size with its relatively large specific surface area helps the occurrence of crystallization and thus decreases the crystallization temperature. [27]The details of this mechanism will be introduced later in this chapter.

However, it is not possible to see from this traces the difference between the crystallization temperature of the two different phases. It was expected to see a lower crystallization temperature for Diopside and a higher one for Wollastonite[18]. This two temperatures are probably too close to be detected by the device.

Moreover, it is possible to observe from these traces how the flux lowered the glass transition temperature, the difference is about 20 degrees.

4.2 Shrinkage evaluation and HSM results.

After this preliminary analysis, the heating treatments were carried out for shrinkage evaluation.

The tables below (Table 4-2,Table 4-3) show the results of this evaluation.

Table 4-2: Axial (ΔS%), radial (ΔD%) and volumetric (ΔV%) shrinkage evaluation for WD + flux at the three different heat treatments.

	Printed tablets			**Pressed tablets**								
	45-100 μm			45-100 μm			25-45 μm			<25 μm		
	ΔS%	ΔD%	ΔV%	ΔS%	ΔD%	ΔV%	ΔS%	ΔD%	ΔV%	ΔS%	ΔD%	ΔV%
775°C	18,5	20,7	48,8	10	13,7	33	11,7	16,6	38,5	15,7	18,7	44,3
800°C	19,3	25,8	55,6	9,6	15,3	35,2	10,3	17,9	39,6	18,5	19,9	47,7
825°C	21,8	26	57,2	0,8	18,2	33,7	6,6	19	38,7	12,4	20,2	44,2

Table 4-3: Axial (ΔS%), radial (ΔD%) and volumetric (ΔV%) shrinkage evaluation for WD eutectic at the three different heat treatments.

	Printed tablets			**Pressed tablets**								
	45-100 μm			45-100 μm			25-45 μm			<25 μm		
	ΔS%	ΔD%	ΔV%	ΔS%	ΔD%	ΔV%	ΔS%	ΔD%	ΔV%	ΔS%	ΔD%	ΔV%
800°C	17,1	21,9	49,6	8,62	13,3	31,4	11,9	17	39,4	12,9	19,3	43,2
900°C	24,4	27	59,8	7,3	14,6	32,4	13,6	17,8	41,6	16,2	19,6	45,8
110°C	23,9	26,9	59,3	9,9	14,1	33,6	11,8	18,1	40,8	12,7	19,8	43,9

It is easy to notice that in every case axial and radial shrinkages (ΔS% and ΔD% respectively) are different, which means that the behavior of both materials is non-isotropic. For both compositions, as well, the shrinkage for printed tablets is quite higher copmpared to pressed tablets and this happens because of the higher porosity of the starting structure. The green samples coming from the printing process, indeed, are far more porous than the pressed samples, as it will be shown later with density and porosity results.

In general, the behavior of the two materials is similar and the shrinkage increases with increasing temperature for the biggest and the medium particle size distributions but not for the smallest one. This is related to the already mentioned process of crystallization that takes place simultaneously with sintering. While sintering, the particle's surface energy is the driving force and the viscous flow is the kinetic path through which the surface area is minimized but when crystallization takes place the crystallized surface of the particle does not flow, slowing down the sintering kinetics. While the driving force of sintering is almost temperature independent, the driving force for crystallization depends to a great extent on temperature (thermally induced process). For this reason it is of essential importance to find the correct heat treatment in order to balance the development of both sintering and crystallization as if one mechanism surrounds the other, the resulting material would not meet the requirements of a glass-ceramics. Indeed, if the sintering overcomes the crystallization process the resultant material will be dense but not enough crystallized and, on the contrary side, if the crystallization is the main process the material will have an unacceptable degree of porosity.

Furthermore, the hot stage microscopy analysis was performed to check the shape maintenance of the materials under the heating treatments.

The tables below show the changes in cross-section area of the samples in HSM. Pictures were taken at the three temperatures corresponding to the different heat treatments carried out for the previous observations.

Table 4-4: HSM cross section images of WD+ flux under heating treatment.

	RT	775°C	800°C	825°C
45-100μm				
25-45μm				
<25μm				

As far as the composition with flux is concerned it is clear that at the temperature of 775°C the shape does not change in a relevant way for all the particle size distribution. Crystallization, indeed, according to the DTA results, does not occur below the temperature of about 880°C. Starting from 800°C some differences can be noted. The shape changes in all cases but for the smallest particle size distribution the cross-area reduction is much higher than the others sizes. At the temperature of 825°C this difference is even more visible. These changes occur even below the crystallization temperature in all likelihood because the heating rate in this case is different from the one used for DTA analysis. Indeed, while for DTA the rate was 10°/min, in this heat treatment the rate was 5°/min. Anyway, thiese results conform to shrinkage evaluation above described: the smallest particle size distribution shows more emphasized shrinkage.

In the second table (Table 4-5)where the results for the eutectic composition are showed, it can be observed that, similarly to the other composition, at the temperature of 800°C the shape doesn't change so much. That temperature, in fact, is not enough to start the sintering process. Instead, at the temperature of 900°C all the three samples show relevant shape change and that shrinkage is much higher in the case of particle smaller than 25 μm.

The main difference between the two materials is that for the eutectic composition the raise of temperature from 900°C to 1100°C does not correspond to a further shrinkage or shape change since once the material is completely crystallized shape changes do not occur anymore.

From these observation, it can be hypothesized that at the temperature of 900°C the eutectic composition is fully crystallized while crystallization does not occur or is not completed for the composition with flux at the temperature of 825°C. XRD analysis was then performed to prove the presence of crystal phases in the heat treated samples. These results will be showed hereunder.

Table 4-5: HSM cross section images of WD eutectic under heating treatment.

	RT	800°C	900°C	1100°C
45-100µm				
25-45µm				
<25µm				

Before choosing the suitable heat treatment for both materials, some scaffolds were printed to check the shape maintenance. The table below (Table 4-6) shows pictures of the scaffolds after every heat treatment.

It can be seen in these pictures that in almost all cases the shape is fairly maintained. The only sample that has significantly lost the shape is the one made with WD + flux and treated at 825°C. This happens because the added flux in this composition leads too much and too early to the formation of a liquid phase during heating. As a results, the viscous flow before crystallization is definitely too high and, as already mentioned, the final part does not fulfill the requested features for geometry and mechanical strength.

Table 4-6: Pictures of scaffolds after every heat treatment.

	775°C	800°C	825°C
WD+flux	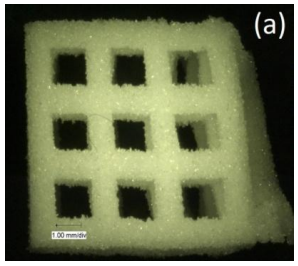	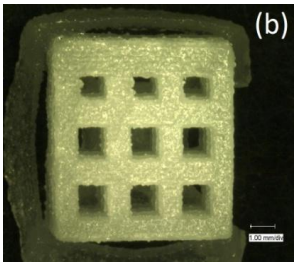	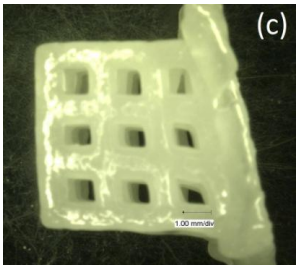
	800°C	**900°C**	**1100°C**
WD eutectic	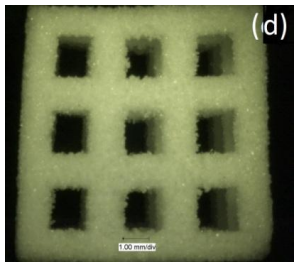	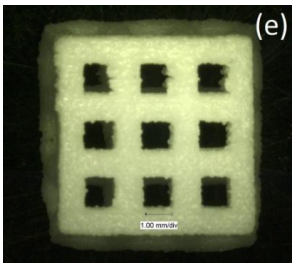	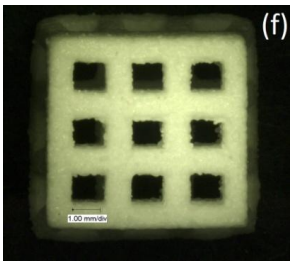

Since the main aim of this entire work is to check if the material is suitable for biomedical applications, besides bioactivity and biodegradability tests, it has been important to take into account the eventual shape of the scaffolds as well. It is even clearer, from Figure 4-2, that for WD + flux, the treatment at 825°C does not allow enough shape maintenance and doesn't definitely fit with the goal of biomedical applications. Therefore, from this result it was already possible to state that it did not make sense to carry out further experiments with the treated material at 825°C.

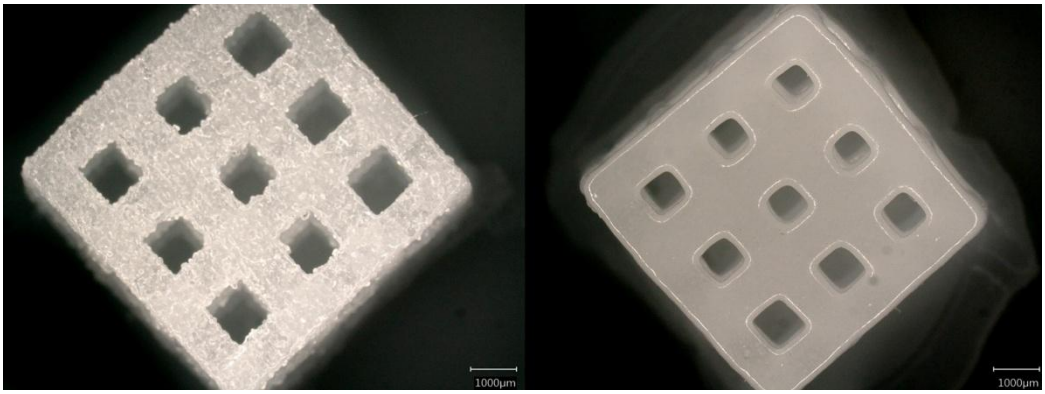

Figure 4-2: Comparison of WD+flux scaffolds treated at 800°C (left) and 825°C (right).

It has been decided to test bioactivity and degradation for the material after the 800°C treatment even if not crystalline to check at least the behavior as bioglass.

Further experiments, then, have been carried out with the glass-ceramic composition with flux after the heat treatment at 800°C and with the eutectic composition after the 900°C treatment.

4.3 Density measurements

Density measurements with Archimede's method was carried out for both materials and every heating treatment. The tables below show the results of this analysis.

Table 4-7: Apparent solid density and bulk density for WD + flux. Highlighted are the values for the chosen heat treatment. Values in [g/(cm^3)]

	775°C		800°C		825°C	
	$\rho_{apparent}$	ρ_{bulk}	$\rho_{apparent}$	ρ_{bulk}	$\rho_{apparent}$	ρ_{bulk}
Printed tablets	2,84 ± 0,013	2,44 ± 0,002	2,80 ± 0,005	2,76 ± 0,010	2,81 ± 0,003	2,76 ± 0,005
Pressed tablets 45-100µm	2,80 ± 0,002	2,61 ±0,023	2,79 ± 0,004	2,77 ± 0,004	2,83 ± 0,001	2,80 ± 0,001
Pressed tablets 25-45µm	2,82 ± 0,004	2,79 ±0,021	2,83 ± 0,001	2,81 ± 0,008	2,86 ± 0,004	2,84 ± 0,005
Pressed tablets <25µm	2,84 ± 0,016	2,79 ± 0,021	2,85 ± 0,010	2,81 ± 0,012	2,90 ± 0,012	2,84 ± 0,031

Table 4-8: Apparent solid density and bulk density for WD eutectic. Highlighted are the values for the chosen heat treatment.

	800°C		900°C		1100°C	
	$\rho_{apparent}$	ρ_{bulk}	$\rho_{apparent}$	ρ_{bulk}	$\rho_{apparent}$	ρ_{bulk}
Printed tablets	2,86 ± 0,027	2,41 ± 0,17	2,83 ± 0,003	2,78 ± 0,02	2,85 ± 0,01	2,8 ± 0,02
Pressed tablets 45-100 µm	2,8 ± 0,01	2,75 ± 0,01	2,82 ± 0,002	2,79 ± 0,01	2,83 ± 0,001	2,8 ± 0,004
Pressed tablets 25-45 µm	2,84 ± 0,01	2,81 ± 0,01	2,85 ± 0,01	2,83 ± 0,003	2,9 ± 0,01	2,85 ± 0,001
Pressed tablets <25µm	2,85 ±0,01	2,81 ± 0,02	2,88 ± 0,003	2,82 ± 0,02	2,9 ± 0,01	2,85 ±0,01

These tables point out that the bulk density is always smaller than the apparent solid density according to the fact that the bulk volume takes into account not only the solid volume and

the closed porosity but also the open porosity. Therefore, bulk volume is bigger than the apparent solid one giving a smaller values of density

As with the Archimedes methods it is not possible to avoid taking into account the closed porosity and the real density (free-pore material) of the two materials was also measured. In this case, the measure was done only for printed and pressed tablets after the two previously decided heat treatments. In the following table values of real density are showed.

Table 4-9: Real density measured with pycnometer for both materials before (parent glass) and after (printed and pressed tablets) heat treatment.

	Parent glass	Pressed tablets	Printed tablets
WD + flux 800°C	2,84 g/cm^3	2,89 g/cm^3	2,89 g/cm^3
WD eutectic 900°C	2,85 g/cm^3	2,99 g/cm^3	2,99 g/cm^3

Comparing these values of real density with the previous measured values of density it can be seen that the measurement with helium pycnometer gives higher results according to the fact that the real density does not take into account open or closed porosity.

Another evidence from pycnometer analysis is that for the WD+ flux composition, the heat treatment does not correspond to a relevant increase of density while values for the eutectic composition are higher after the treatment. This result accords to the conclusion that for the composition with flux the treatment at 800°C does not lead to crystallization differently from the eutectic composition at 900°C.

Starting from density values, with Archimede's method and with the pycnometer, it has been possible to evaluate apparent and total porosity. Closed porosity was easily calculated as difference of the total and apparent ones. Values are referred to printed and pressed values as Archimede's method was carried out on tablets. The following table (Table 4-10) shows all porosity values.

Table 4-10: Values of apparent, total and closed porosity for both materials.

		Apparent porosity	Total porosity	Closed porosity
WD + flux	Printed tablets	1,45%	4,62%	3,17%
	Pressed tablets	0,92%	4,18%	3,26%
WD eutectic	Printed tablets	1,83%	7,06%	5,23%
	Pressed tablets	1,03%	6,79%	5,76%

The most important evidence here is the difference between the values of total porosity of the two materials. The eutectic composition shows values higher of two percentage points than the other composition probably due to the crystallization process.[28]

Another observation to be done is about the different manufacturing process: in the same way for both materials the printing process induces grater total porosity than the pressing procedure.

4.4 XRD analysis

To check the crystalline phases in all materials after the heat treatment XRD analysis was carried out. The figures below show the obtained diffraction patterns.

In Figure 4-3, concerning the composition with flux, no relevant peaks are visible confirming that the heat treatment at 800°C for this composition is not enough to induce the crystallization process.

The three broad peaks that appear, probably lead to the presence of some crystallized areas that cannot be associated with a specific phase.

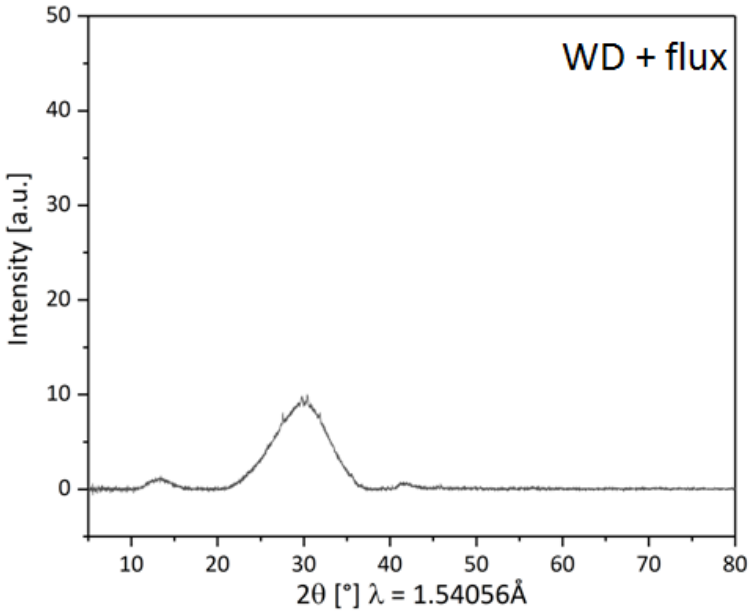

Figure 4-3: XRD pattern for WD + flux after 800°C heat treatment.

The second image (Figure 4-4) shows the result for the eutectic composition.

In this case, differently from the previous one, many peaks are visible and as it was expected, the peaks of Diopside and Wollatonite are present confirming that the crystallization process has took place.

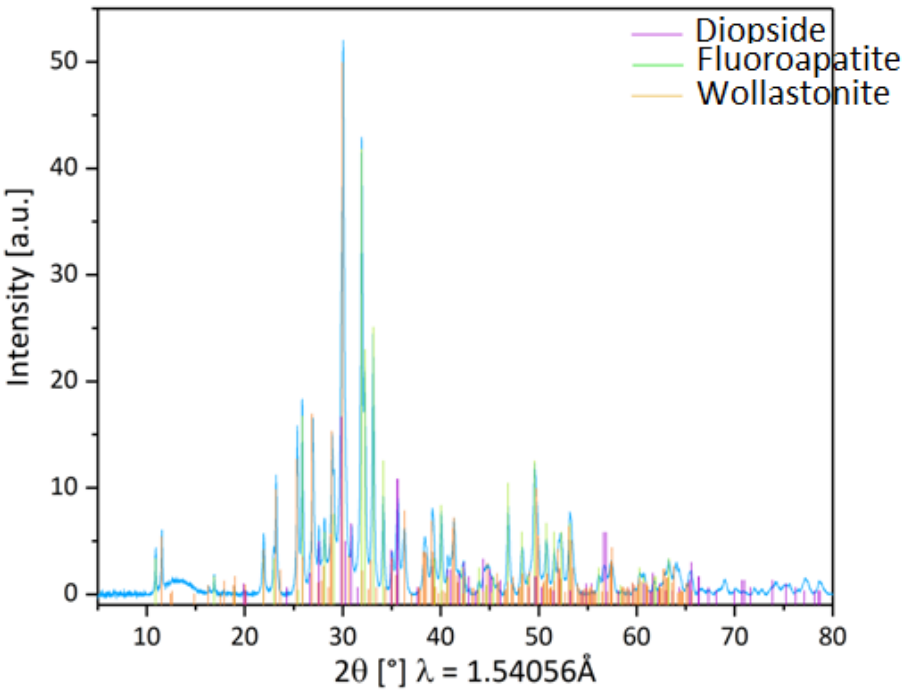

Figure 4-4: XRD pattern for WD eutectic after 900°C heat treatment.

The XRD analysis was carried out for WA glass-ceramic as well to verify the presence of the two required phases as this material has been made *ad hoc* in these experiments.[2] The analysis confirmed the correct crystallization of both phases. The figure below (Figure 4-5) shows the diffractogram for this material and the peaks of wollastonite and hdroxyapatite are clearly noticeable.

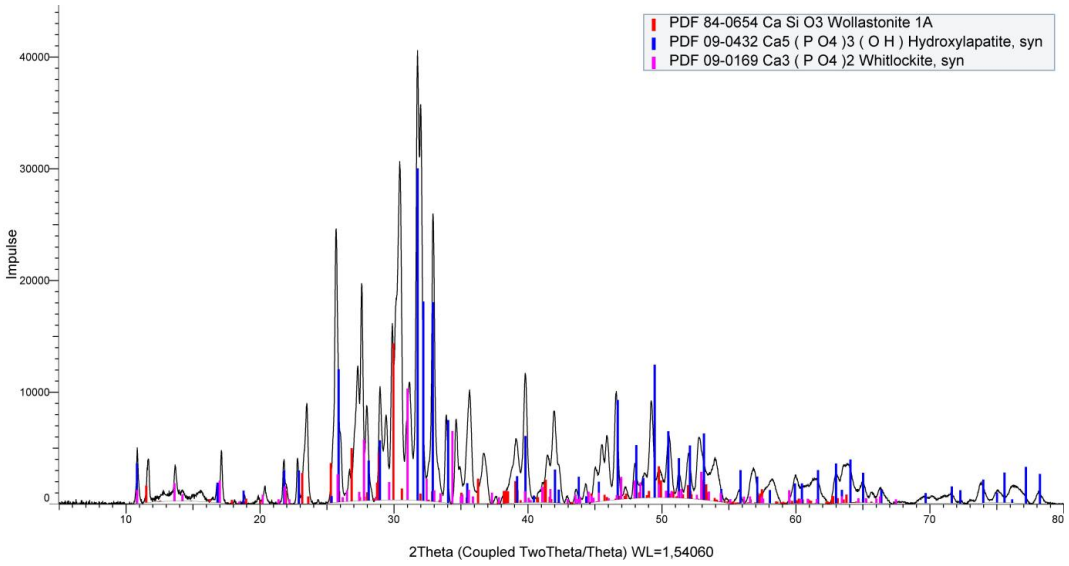

Figure 4-5: XRD pattern for WA glass-ceramic after 1050°C heat treatment.

4.5 Mechanical characterization

The table below shows the results of B3B test.

Table 4-11: Values of Weibull modulus and σ_0 in case of pressed and printed tablets for both materials.

	WD flux pressed	WD flux printed	WD eutectic pressed	WD eutectic printed
m	5,88	5,5	19,54	13,8
σ_0(MPa)	121,44	83,8	137,21	98,57

It can be seen that, in case of pressed tablets, the values of characteristic strength are always higher than the values of printed tablets. This evidence can be explained considering that the final porosity of printed tablets is higher than the pressed ones. Indeed, the higher porosity of the printed tablets increases the probability to find cracks long enough to cause earlier the brittle fracture as the failure stress is inversely proportional to the crack length.

Another relevant observation is to be made between the two compositions: the eutectic tablets show, both in case of pressed and printed components, higher values compared to the other composition according to the fact that the first material, with the adopted treatment, is subject to crystallization while the last one does not crystallize at the temperature used in the present experiments. Mechanical properties of a crystalline material are by nature higher than those of an amorphous one.

Another thing observed during mechanical measurements was the correlation between fracture pieces and strength values: number of pieces increased with values of failure stress. This is probably linked to creation of a higher amount of fracture surface requiring higher stresses.

Values of Weibull modulus[3] for the eutectic composition are considerably high since typically *m* values for ceramic materials are within the range [5-15]. It is stated in other studies that high values of Weibull modulus reflect the advanced technological stage of fabrication and processing of ceramic-based material for biomedical applications.[29]

All these results confirm that the idea to employ glass-ceramics instead of glasses for load-bearing application could have good matches.

The values of the previous table were exitimated by the Weibull approach to brittle materials and the following image shows the Weibull plots.

All the plots confirm that the assumption of a Weibull distribution is reasonable and fits well the data from mechanical tests as they are in each case nearly linear and there are no outliners.

[3] Weibull modulus, as mentioned in the previous chapter, is a measure of data scatter and therefore of the material's reliability.

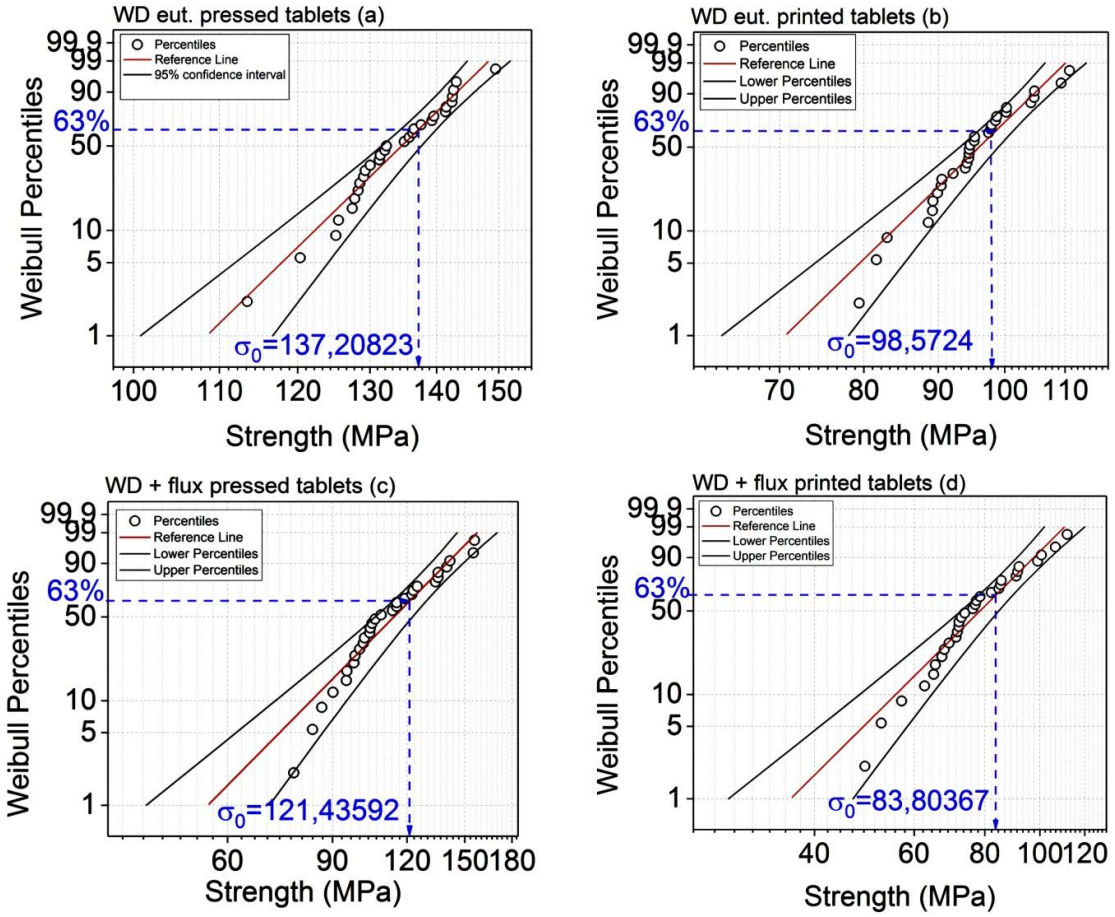

Figure 4-6: Weibull plots of mechanical tests on pressed and printed tablets of both compositions.

4.6 Degradation and bioactivity tests

Degradation analysis of the specimens is, together with SBF tests, an important step to be done before any other clinical study. As already stated in the introduction, the main goal in bone tissue engineering is to find a material with the proper combination of bioresorbability and bioactivity. In particular, if the material shows the appropriate degree of dissolution, resorption will reasonably take place.

In the following image (Figure 4-7) the trend of ions analyzed during the 8 weeks testing period is shown.

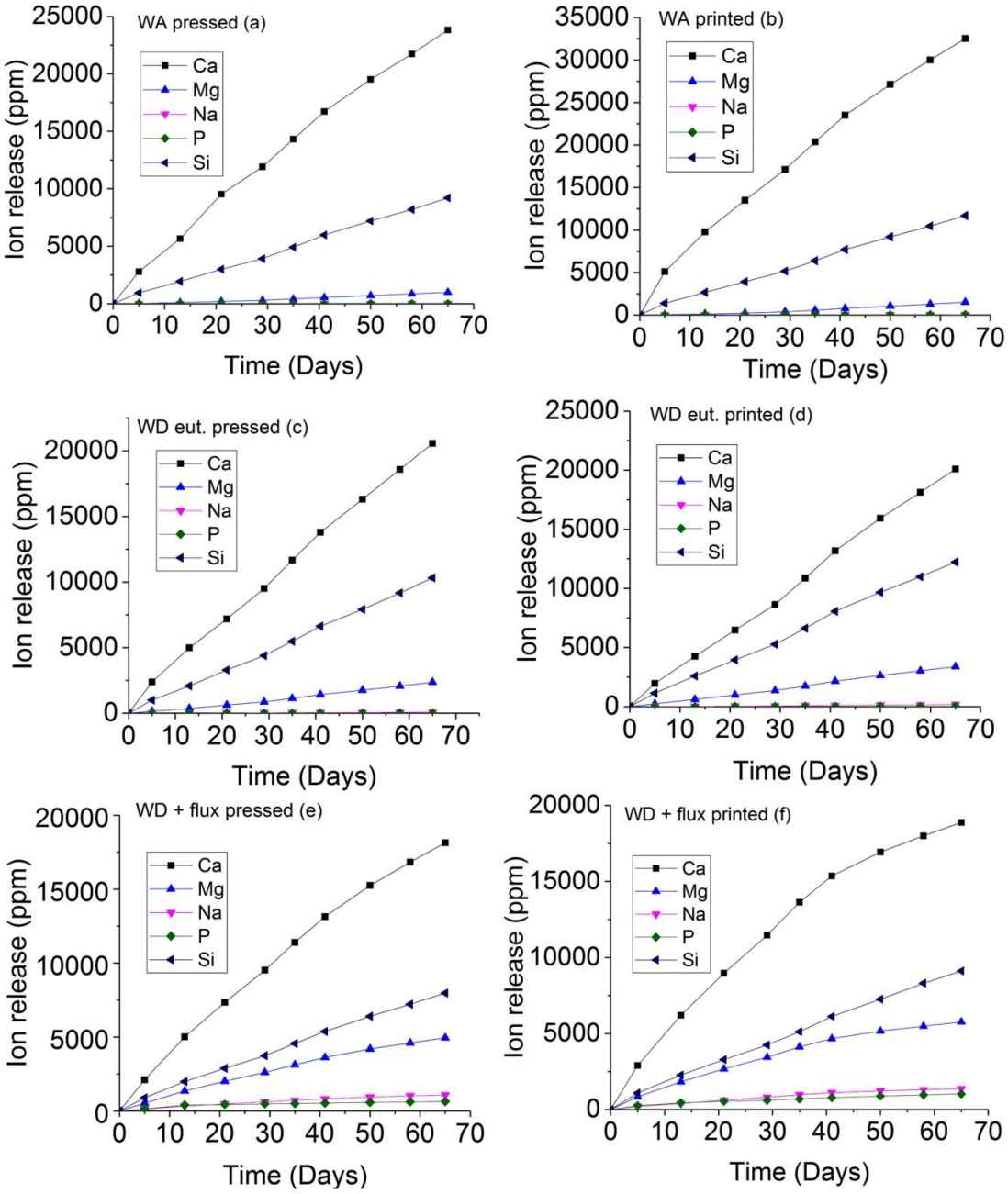

Figure 4-7: Overall plot of degradation test.

The main evidence here is that, the release of calcium and magnesium ions has a similar fashion for both WD materials as it has the WA glass-ceramic used as standard. The evolution if ions in case of WA glass-ceramic reproduces quite accurately results obtained in other studies[30] confirming the reliability of this comparison. Release of phosphorus is negligible in case of WA glass-ceramic while it is relevant in the other two cases due to the different composition of WD glass-ceramics. Then, observing plots of WD glass ceramics it is clear that for the one with the sodium-phosphate flux added it is not negligible the release of sodium besides calcium, magnesium and phosphorus.

It is also newsworthy in this study to compare the behavior between printed and pressed tablets. For all materials the higher porosity linked to the printing process (and in particular the apparent porosity) leads to higher values of ion release probably owing to a greater rate of diffusion recognized as controlling the mechanism of dissolution.
This results confirms the idea that printed structures show a good potential in bone tissue engineering applications.

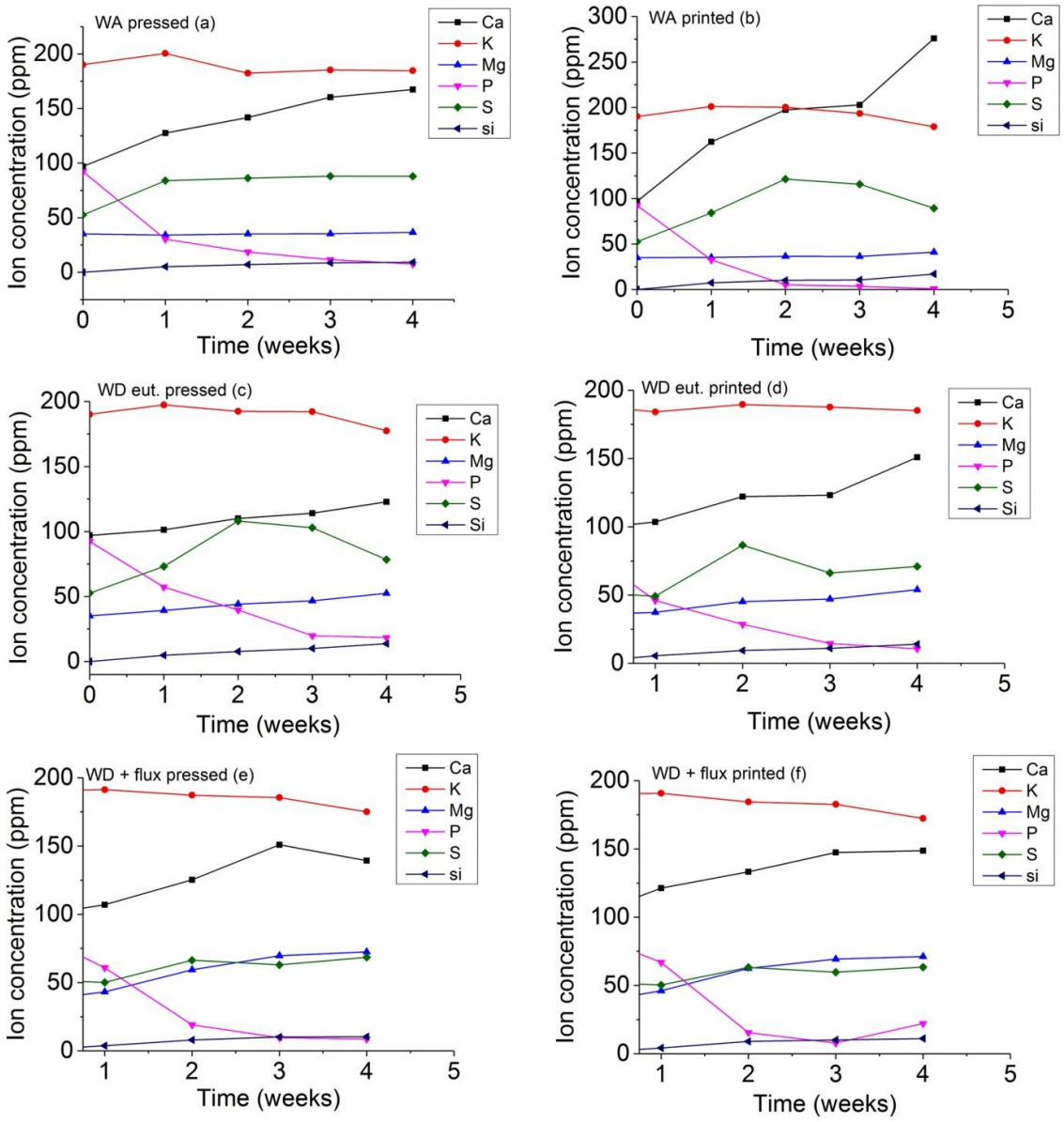

Figure 4-8: Overall plot of bioacitivity test.

The release profiles of Ca, Mg and P of WA glass-ceramic and WD materials show the same fundamental features; in particular, it can be observed that, differently from other ions, amount of phosphorus in the solution decreases from the beginning. This evidence can be

reasonably linked to the mechanism of a Ca-P phase precipitation on the surface of the soaked samples. This explanation can be given on the basis of previous studies carried out on materials similar to the ones analyzed in the present work. Indeed, it has been demonstrated that materials belonging to the wollastonite-diopside system show an analogous trend in ions variation in a SBF solution.[31]
Only in case of printed, WD + flux tablets it can be seen a slight raise in P amount in the solution in the last stages of the analysis. This is probably due to the higher amount of P in the starting material and the higher amount of porosity compared to the pressed tablets allowing a greater interaction between solution the material.

Another observation to be done is that Ca release doesn't show (except in case of WD with flux composition) a slope change correspondingly to the apatite-like layer due to the continuous dissolution if it from the sample.

4.7 SEM surface characterization

Results of SEM/EDX analysis are shown below.

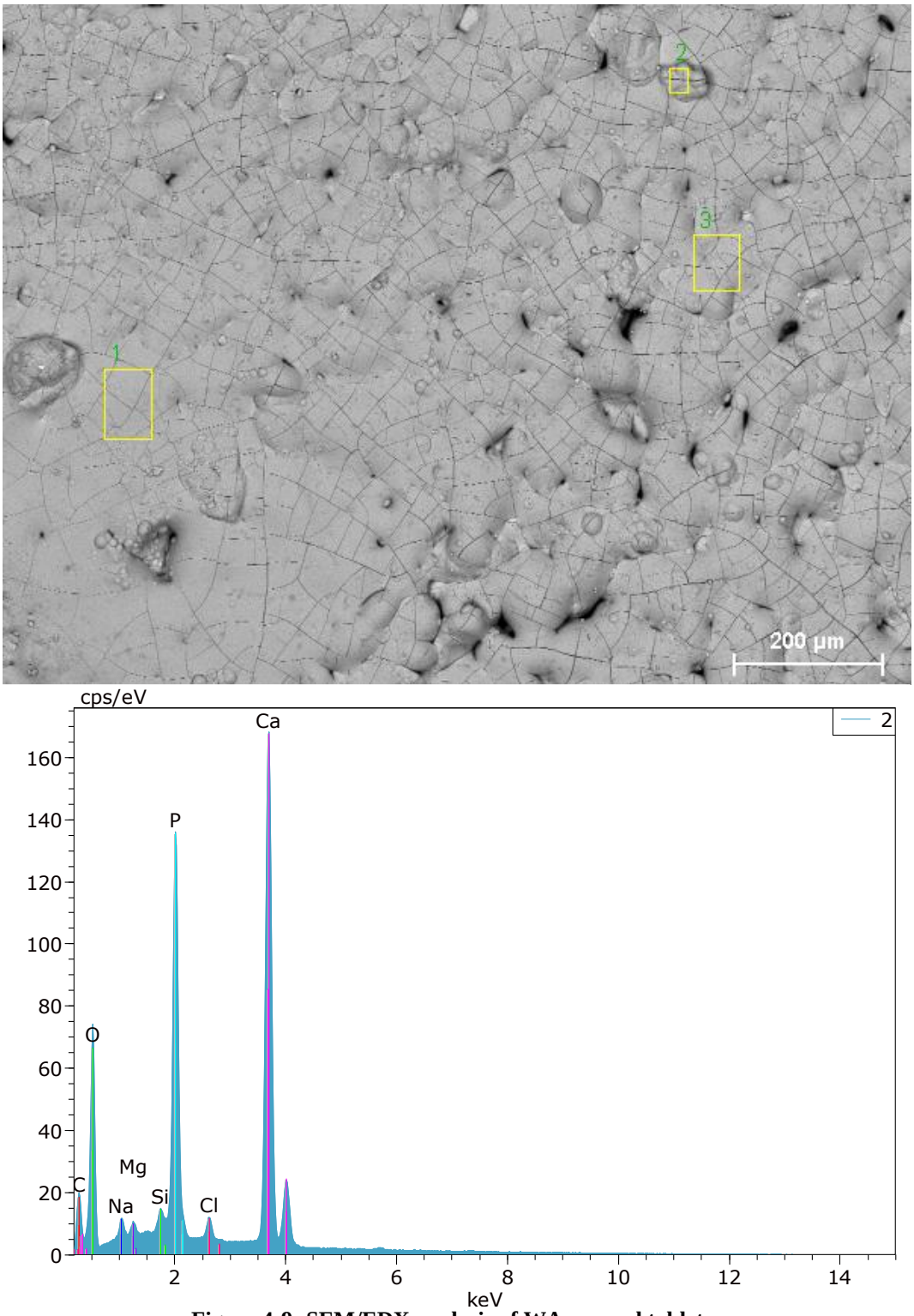

Figure 4-9: SEM/EDX analysis of WA pressed tablets.

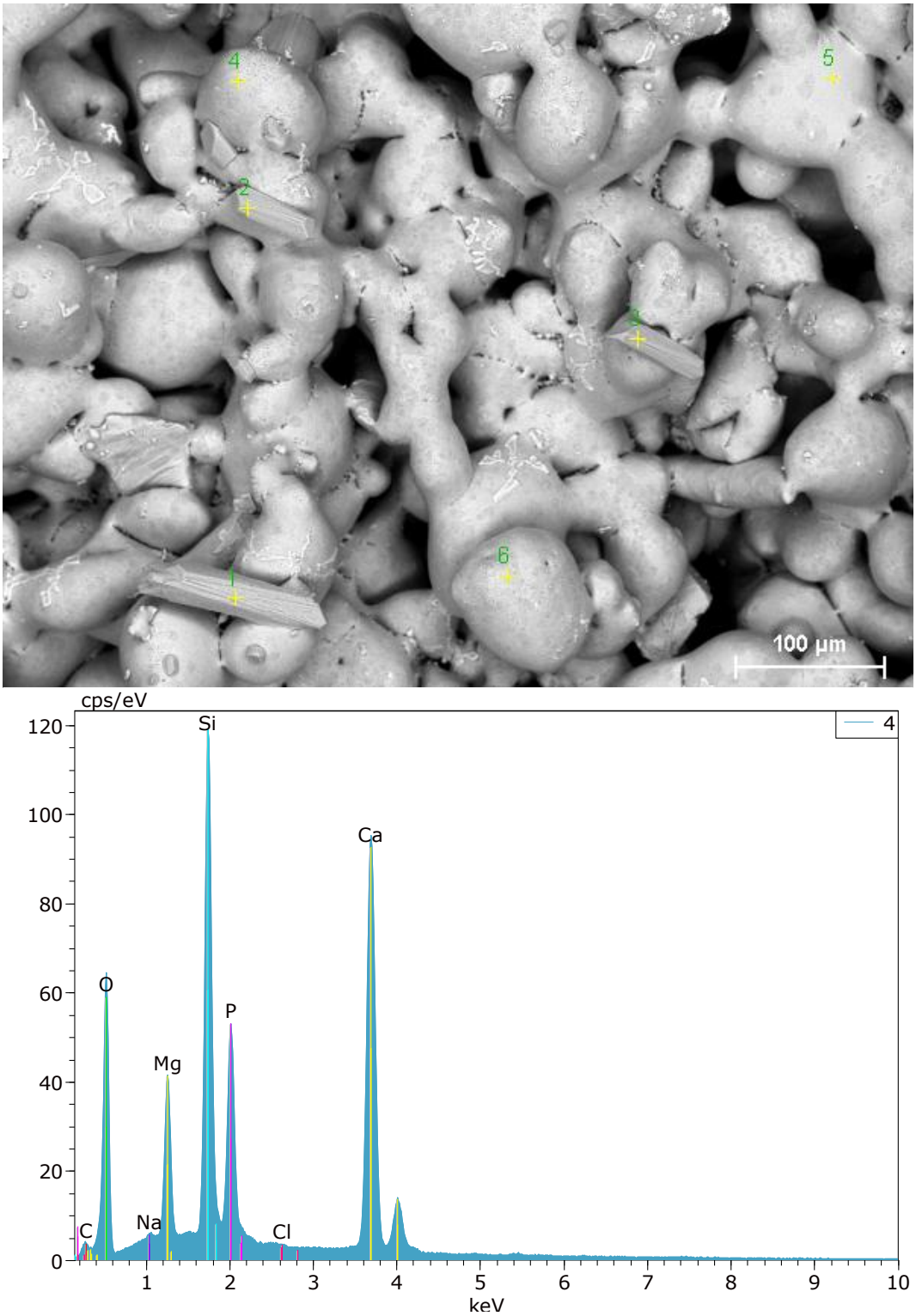

Figure 4-10: SEM/EDX analysis of WA printed tablet.

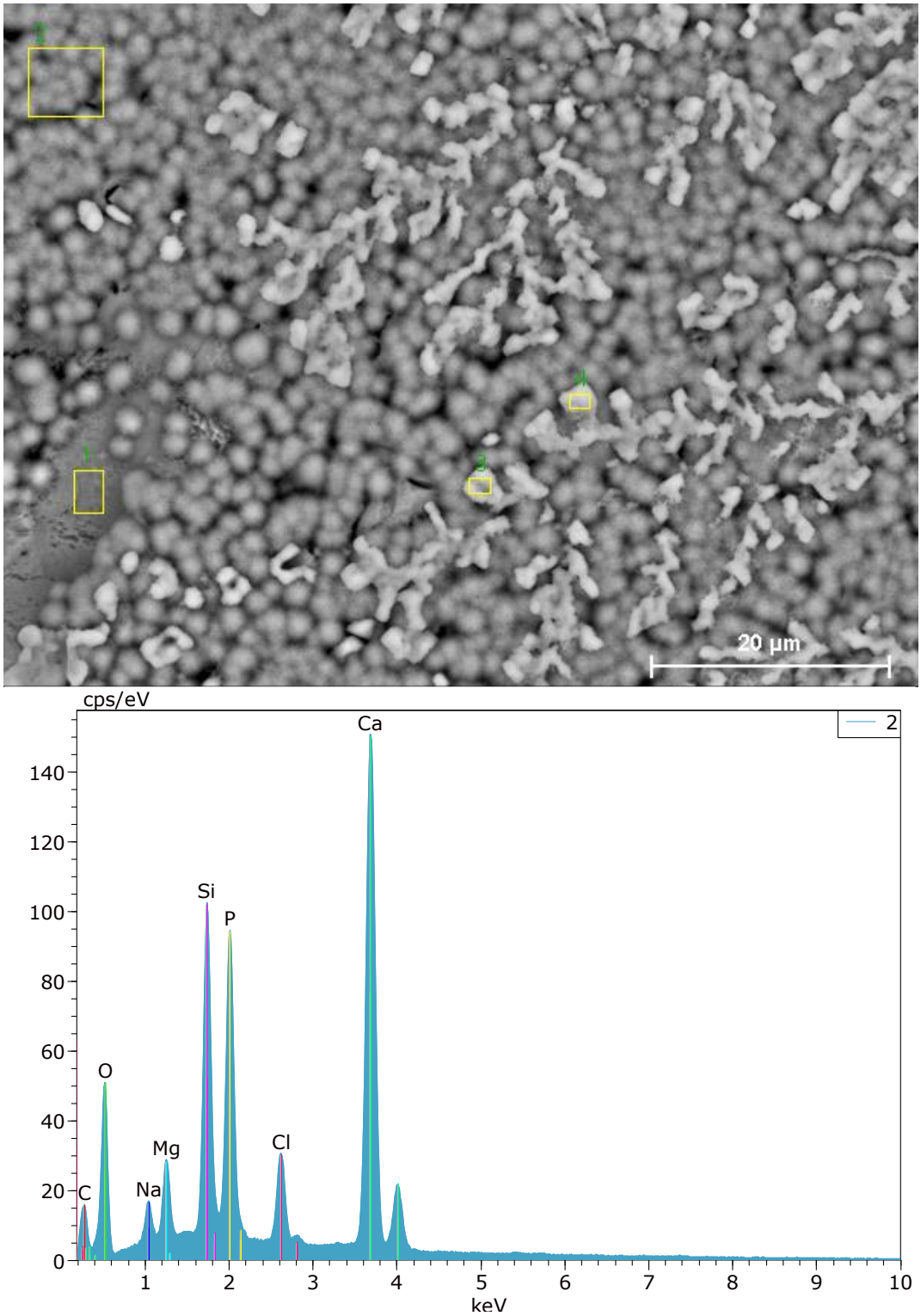

Figure 4-11:SEM/EDX analysis of WD eutectic pressed tablet.

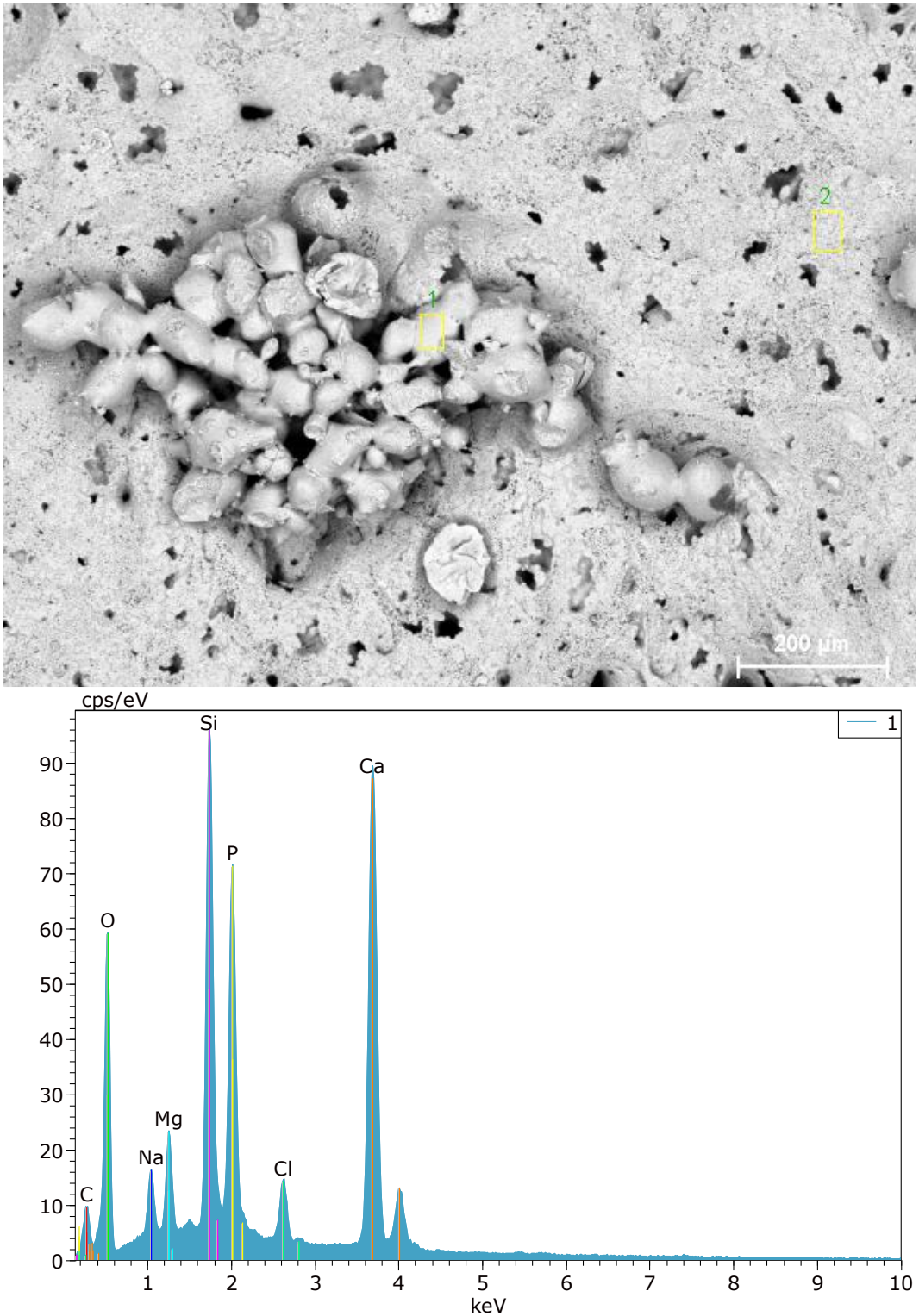

Figure 4-12:SEM/EDX analysis of WD eutectic printed tablet.

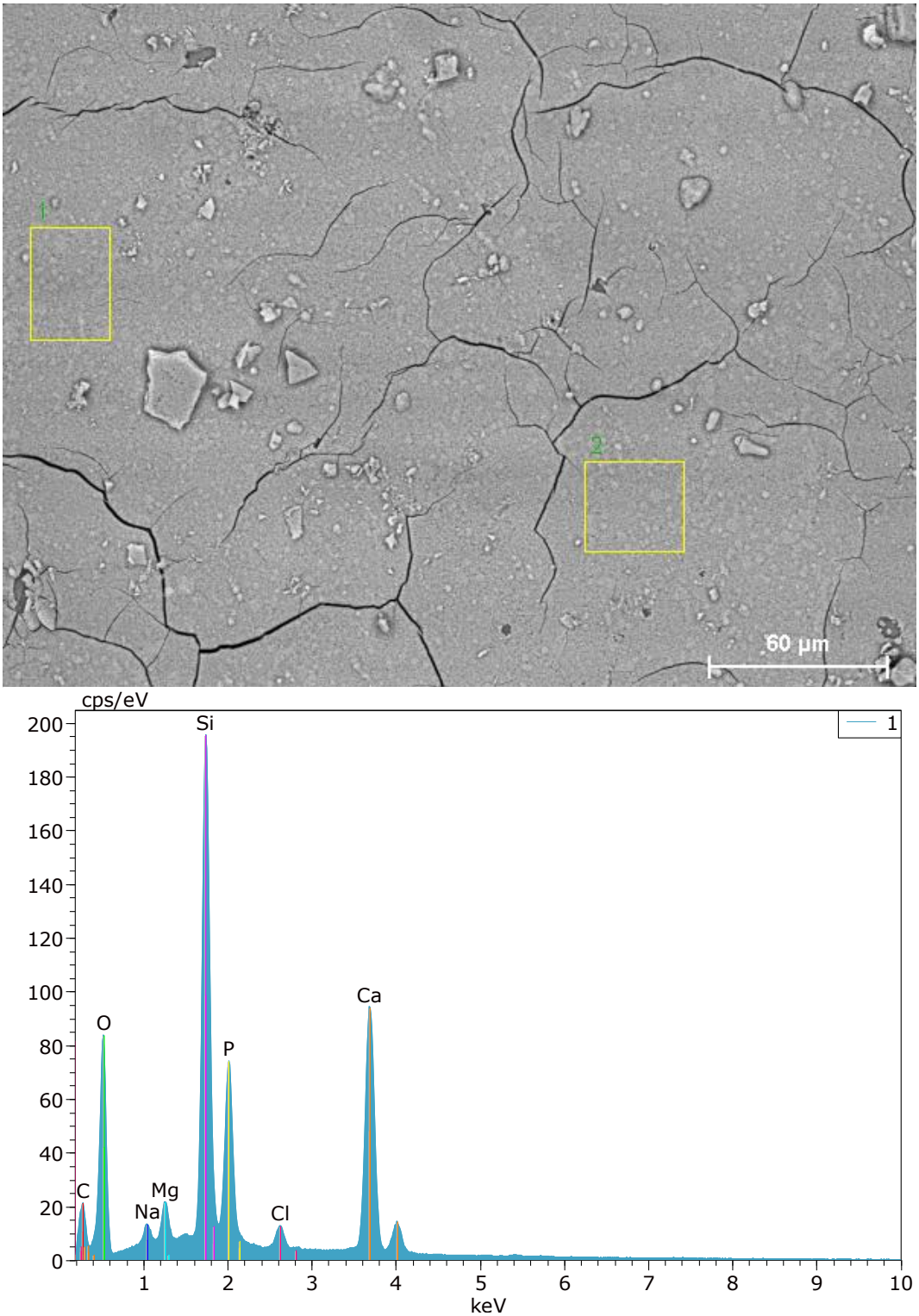

Figure 4-13: SEM/EDX analysis of WD+ flux pressed tablet.

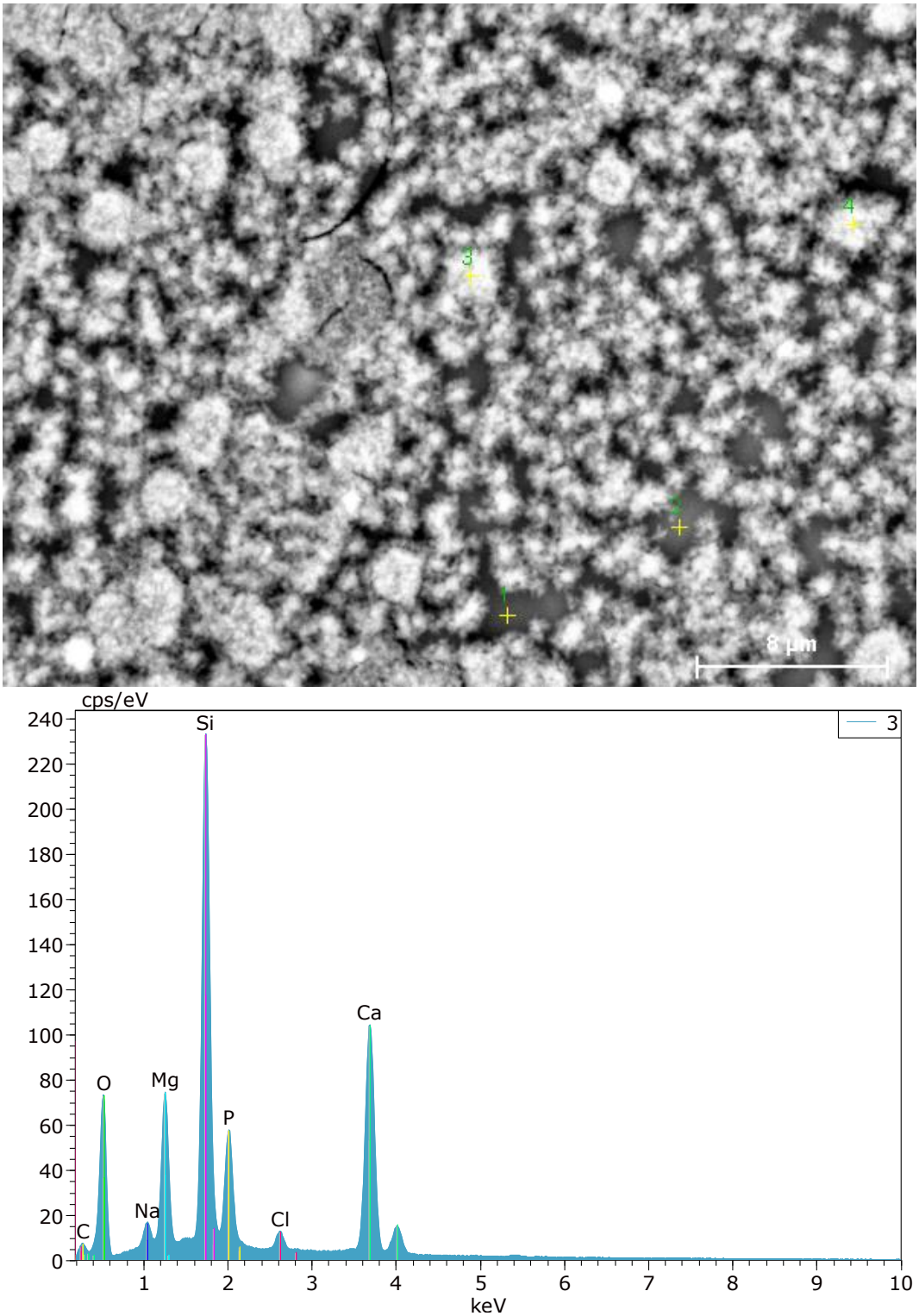

Figure 4-14: SEM/EDX analysis of WD + flux printed tablet.

This last surface analysis did not show completely satisfactory results mainly because, in the EDX spectra, most of the Ca:P ratios did not reproduce exactly the value of 1,667 expected for hydroxyapatite[32]. This is probably due to difficulty to sunder signals coming from the surface layer and the substrate rich in calcium. Results are always polluted by Ca; values of the ratio are, in fact, always higher than expected.

WA glass-ceramic shows values of Ca:P ratio close to the theoretical ones as expected,

especially the printed tablet (Figure 4-10) owing to a greater growth of the layer that allows results not to be contaminated by the substrate.
Moreover, confirming the correct behavior of WA glass-ceramic, the morphology of the surface layer reflects perfectly morphologies already found out in other studies. [33]
It is to be noted also that the eutectic composition of WD glass ceramic shows a close value of this ratio to the theoretical one suggesting that the layer on the surface is really hydroxyapatite. (The EDX spectrum in Figure 4-11 is referred to the box N° 2 placed on the top-left corner of the SEM image).
Moreover, it is clear from Figure 4-11 and Figure 4-14 that the surface layer growing on the WD tablets is not compact meaning that growth of the layer is slower for the analyzed materials than in case of the standard one.

Another relevant observation to be done is on Figure 4-12: it can be seen that morphology of the structure growing on the surface resembles the one observed in case of WA glass-ceramic suggesting again that the behavior of WD eutectic glass ceramic is similar to the one of the standard material. Such a structure hasn't been found for WD + flux composition leading to think that bioactivity of this material is lower that for the eutectic material.

One last relevant evidence comes from where it can be recognized the needle-like shape of the growing layer expected on the basis of other studies[34]. The image is referred to WD eutectic glass-ceramic confirming once again the good bioactive behavior of this material.

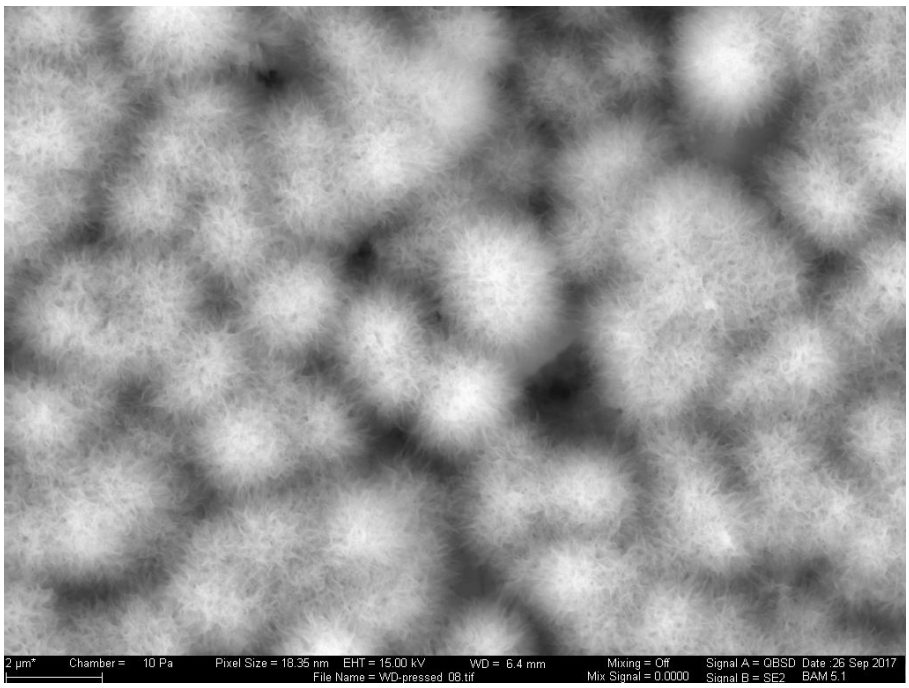

Figure 4-15 : Detail of surface of WD eutectic glass-ceramic.

It is to be said that the SEM/EDX analysis is not enough to claim that the layer growing on the surface is for sure hydroxyapatite meaning that, even if these last results are not fully satisfying, they are anyway essential while studying bioactivity.

Conclusions

It has been demonstrated, accordingly to the hypothesis, by the present work, that the use of a glass-ceramic in biomedical fields is effectively a good choice and in particular for load-bearing applications as mechanical properties are higher than in case of amorphous materials such as the Bioglass®.

The composition with the flux didn't show an acceptable trade-off between crystallization and shape maintenance, thus, limiting its potential use in biomedical, load bearing applications.

On the other side, the eutectic composition showed a better crystallization behavior always maintaining a good shape. Indeed, mechanical properties where always higher than for the other composition due to the high amount of crystalline phase.

With regards to the second part of the work, both compositions of WD glass-ceramic showed good degradation and bioactive behaviors making them interesting in bone tissue engineering field and, as far as the composition with flux concerns, it could be potentially used in applications that do not involve great stresses.

As mentioned in the very last rows of chapter 4, the SEM/EDX analysis resulted no to be enough to characterize the layer growing on the surface of the sample. It cuold be stated with enough confidence that such a layer is made by hydroxyapatite comparing its morphology to the one of the layer growing on the standard material
Further analysis as, for example, XRD or FTIR spettroscopy could be scheduled to check the effective growth of hydroxyapatite.

XRD analysis was supposed to be carried out on the samples produced during the present study but it wasn't satisfactory as they showed a not completely smooth surface. For this reason such results have been omitted.

Acknowledgements

I want to thank my parents Sergio and Francesca before anyone else.
Without all their sacrifices I would not be here writing these words now. They gave me the possibility to fulfill all my dreams, they showed me the way, they taught me to face life.

Together with my parents I need to thank my two big brothers Davide and Alessandro. I grew up with them and if I am like I am today it is also because of them. They both gave me the joy to be the aunt of two amazing baby boys fruit of the love for their partners Chiara and Valentina.
Furthermore, a special thanks goes to my uncles Ottorino and Ferdinando and to my grandmother Maria, they always encouraged me for every exam and every project during this six years.
A great thanks goes also to all the other uncles, aunts and all my amazing cousins with which I shared a lot of happy moments of my life.

Immediately after the family, I want to thank every single one of my friends. The ones that shared with me "party moments", the ones that shared with me lots of afternoons at the library, the ones that shared with me amazing happy-hours to relax after studying. I know that they will identify reading these words even if I do not call them by name.

Everyone of them owns a piece of my heart.

Special recognition goes to Greta, my soul-mate, and Alessandra, my "life-mate"; they are the demonstration that friends are the family one chooses.

Separate thanks goes to all the guys I met at the university, to all of them that helped me with notes and advices especially the thirteen ones that shared with me a wonderful vacation in Policoro.

Moreover, I would like to express my sincere gratitude for professor Paolo Colombo for his limitless willingness and all the inspiration he gave me.

Throughout my internship I had the opportunity to meet and work with several people, whom I would like to thank sincerely and dedicate the following words.

First of all, my gratitude goes to Jens Gűnster as he gave me this special opportunity of working on a great project with a great team. I want to say thank you to all my colleagues at BAM for all the support they gave me, special thanks goes to Andrea Zocca for all the help and all the advices.

As my time in Berlin was not only made of work, I want to thank all my Berliner friends with a special recognition to my flatmates Juan, Sergio, Oscar and Julia for accepting me and for sharing with me the special experience that living with friends is.

Bibliography

1. Williams, D. F. *The Williams dictionary of biomaterials.* (1999).

2. Kokubo, T. Bioactive glass ceramics: properties and applications. *Biomaterials* **12,** 155–163 (1991).

3. Hench, L. L. The story of Bioglass®. *J. Mater. Sci. Mater. Med.* **17,** 967–978 (2006).

4. Cannillo, V., Colmenares-Angulo, J., Lusvarghi, L., Pierli, F. & Sampath, S. In vitro characterisation of plasma-sprayed apatite/wollastonite glass–ceramic biocoatings on titanium alloys. *J. Eur. Ceram. Soc.* **29,** 1665–1677 (2009).

5. Gu, Y. ., Khor, K. . & Cheang, P. In vitro studies of plasma-sprayed hydroxyapatite/Ti-6Al-4V composite coatings in simulated body fluid (SBF). *Biomaterials* **24,** 1603–1611 (2003).

6. Wilson, J., Pigott, G. H., Schoen, F. J. & Hench, L. L. Toxicology and biocompatibility of bioglasses. *J. Biomed. Mater. Res.* **15,** 805–817 (1981).

7. Mancuso, E. Processing and Characterisation of Novel Bioceramics for Load Bearing Applications by. (2016).

8. Habraken, W., Habibovic, P., Epple, M. & Bohner, M. Calcium phosphates in biomedical applications: materials for the future? *Mater. Today* **19,** 69–87 (2016).

9. Kokubo, T., Ito, S., Shigematsu, M., Sanka, S. & Yamamuro, T. Fatigue and life-time of bioactive glass-ceramic A-W containing apatite and wollastonite. *J. Mater. Sci.* **22,** 4067–4070 (1987).

10. Ohtsuki, C., Kamitakahara, M. & Miyazaki, T. Bioactive ceramic-based materials with designed reactivity for bone tissue regeneration. *J. R. Soc. Interface* **6,** S349 LP-S360 (2009).

11. Yoon, S.-D., Lee, J.-U., Lee, J.-H., Yun, Y.-H. & Yoon, W.-J. Characterization of Wollastonite Glass-ceramics Made from Waste Glass and Coal Fly Ash. *J. Mater. Sci. Technol.* **29,** 149–153 (2013).

12. Wu, C., Ramaswamy, Y. & Zreiqat, H. Porous diopside (CaMgSi2O6) scaffold: A promising bioactive material for bone tissue engineering. *Acta Biomater.* **6,** 2237–2245 (2010).

13. A. De Castro Juraski , A. C. Dorion Rodas, H. Elsayed , E. Bernardo , Vi. Oliveira Soares, J. D. The in vitro bioactivity, degradation and cytotoxicity of Polymer-derived Wollastonite-Diopside Glass ceramics. *Materials (Basel).* (2017).

14. Seitz, H., Rieder, W., Irsen, S., Leukers, B. & Tille, C. Three-dimensional printing of porous ceramic scaffolds for bone tissue engineering. *J. Biomed. Mater. Res. Part B Appl. Biomater.* **74B,** 782–788 (2005).

15. Zhang, H., Ye, X.-J. & Li, J.-S. Preparation and biocompatibility evaluation of apatite/wollastonite-derived porous bioactive glass ceramic scaffolds. *Biomed. Mater.* **4,** 45007 (2009).

16. Xiao, K., Dalgarno, K. W., Wood, D. J., Goodridge, R. D. & Ohtsuki, C. Indirect selective laser sintering of apatite—wollostonite glass—ceramic. *Proc. Inst. Mech. Eng. Part H J. Eng. Med.* **222,** 1107–1114 (2008).

17. Panna, W., Wyszomirski, P. & Kohut, P. Application of hot-stage microscopy to evaluating sample morphology changes on heating. *J. Therm. Anal. Calorim.* **125,** 1053–1059 (2016).

18. Castegini, C. Manifattura additiva di biovetroceramici. (Università degli Studi di Padova, 2016).

19. ISO 18754: Fine ceramics (advanced ceramics, advanced technical ceramics) - Determination of density and apparent porosity. (2013).

20. Viana, M. About pycnometric density measurements. *Talanta* **57,** 583–593 (2002).

21. DIN 66137-1. Determination of solid state density- Part 1: Principles. (DIN 66137-1:2003-11). (2003).

22. Börger, A., Supancic, P. & Danzer, R. The ball on three balls test for strength testing of brittle discs: stress distribution in the disc. *J. Eur. Ceram. Soc.* **22,** 1425–1436 (2002).

23. Lu, C., Danzer, R. & Fischer, F. D. Influence of Threshold Stress on the Estimation of the Weibull Statistics. *J. Am. Ceram. Soc.* **85,** 1640–1642 (2002).

24. Khalili, A. & Kromp, K. Statistical properties of Weibull estimators. *J. Mater. Sci.* **26,** 6741–6752 (1991).

25. ISO 10993-14: Biological evaluation of medical devices- Part 14: Identification and qualification of degradation products from ceramics. (EN ISO 10993-14: 2009). (2009).

26. Kokubo, T. & Takadama, H. How useful is SBF in predicting in vivo bone bioactivity? *Biomaterials* **27,** 2907–2915 (2006).

27. Influence of particle size on the crystallization kinetics of glasses produced from waste materials. *J. Non. Cryst. Solids* **357,** 211–219 (2011).

28. Karamanov, A. & Pelino, M. Induced Crystallization Porosity and Properties of Sintereds Diopside and Wollastonite glass–ceramics. *J. Eur. Ceram. Soc.* **28,** 555–562 (2008).

29. Wendler, M. *et al.* Chairside CAD/CAM materials. Part 2: Flexural strength testing. *Dent. Mater.* **33,** 99–109 (2017).

30. Kunjalukkal Padmanabhan, S. *et al.* Wollastonite/hydroxyapatite scaffolds with improved mechanical, bioactive and biodegradable properties for bone tissue engineering. *Ceram. Int.* **39,** 619–627 (2013).

31. Sainz, M. A., Pena, P., Serena, S. & Caballero, A. Influence of design on bioactivity of novel CaSiO3–CaMg(SiO3)2 bioceramics: In vitro simulated body fluid test and thermodynamic simulation. *Acta Biomater.* **6,** 2797–2807 (2010).

32. ISO 13779-3 Implants for surgery- Hydroxyapatite- Part 3: chemical analysis and

characterization of crystallinity and phase purity.

33. Yu, S., Hariram, K. P., Kumar, R., Cheang, P. & Aik, K. K. In vitro apatite formation and its growth kinetics on hydroxyapatite/polyetheretherketone biocomposites. *Biomaterials* **26,** 2343–2352 (2005).

34. Miake, Y. *et al.* High-resolution and Analytical Electron Microscopic Studies of New Crystals Induced by a Bioactive Ceramic (Diopside). *J. Dent. Res.* **74,** 1756–1763 (1995).